Received: 27 March 2019 | Revised: 14 August 2019 | Accepted: 22 August 2019

DOI: 10.1111/jzs.12344

ORIGINAL ARTICLE

JOURNAL OF ZOOLOGICAL SYSTEMATICS AND EVOLUTIONARY RESEARCH

WILEY

A phylogenetically informed search for an alternative *Macrostomum* model species, with notes on taxonomy, mating behavior, karyology, and genome size

Lukas Schärer[1] | Jeremias N. Brand[1] | Pragya Singh[1] | Kira S. Zadesenets[2] | Claus-Peter Stelzer[3] | Gudrun Viktorin[1]

[1]Evolutionary Biology, Zoological Institute, University of Basel, Basel, Switzerland

[2]The Federal Research Center Institute of Cytology and Genetics SB RAS, Novosibirsk, Russia

[3]Research Department for Limnology, University of Innsbruck, Mondsee, Austria

Correspondence
Lukas Schärer, University of Basel, Zoological Institute, Evolutionary Biology, Vesalgasse 1, 4051 Basel, Switzerland.
Email: lukas.scharer@unibas.ch

Funding information
Schweizerischer Nationalfonds zur Förderung der Wissenschaftlichen Forschung, Grant/Award Number: 31003A-143732 and 31003A-162543; Siberian Branch, Russian Academy of Sciences, Grant/Award Number: 0324-2019-0042

Abstract

The free-living flatworm *Macrostomum lignano* is used as a model in a range of research fields—including aging, bioadhesion, stem cells, and sexual selection—culminating in the establishment of genome assemblies and transgenics. However, the *Macrostomum* community has run into a roadblock following the discovery of an unusual genome organization in *M. lignano*, which could now impair the development of additional resources and tools. Briefly, *M. lignano* has undergone a whole-genome duplication, followed by rediploidization into a 2n = 8 karyotype (distinct from the canonical 2n = 6 karyotype in the genus). Although this karyotype appears visually diploid, it is in fact a hidden tetraploid (with rarer 2n = 9 and 2n = 10 individuals being pentaploid and hexaploid, respectively). Here, we report on a phylogenetically informed search for close relatives of *M. lignano*, aimed at uncovering alternative *Macrostomum* models with the canonical karyotype and a simple genome organization. We taxonomically describe three new species: the first, *Macrostomum janickei* n. sp., is the closest known relative of *M. lignano* and shares its derived genome organization; the second, *Macrostomum mirumnovem* n. sp., has an even more unusual genome organization, with a highly variable karyotype based on a 2n = 9 base pattern; and the third, *Macrostomum cliftonensis* n. sp., does not only show the canonical 2n = 6 karyotype, but also performs well under standard laboratory culture conditions and fulfills many other requirements. *M. cliftonensis* is a viable candidate for replacing *M. lignano* as the primary *Macrostomum* model, being outcrossing and having an estimated haploid genome size of only 231 Mbp.

KEYWORDS
genome evolution, karyology, phylogeny, taxonomy, Turbellaria

1 | INTRODUCTION

The free-living flatworm *Macrostomum lignano* Ladurner, Schärer, Salvenmoser, Rieger 2005 (Rhabditophora, Macrostomorpha) has emerged as a model for a broad range of research topics (Ladurner, Schärer, Salvenmoser, & Rieger, 2005), including the biology of aging (Mouton, Grudniewska, Glazenburg, Guryev, & Berezikov, 2018; Mouton et al., 2009), bioadhesion (Lengerer, Hennebert, Flammang, Salvenmoser, & Ladurner, 2016; Lengerer et al., 2014; Wunderer et al., 2019), regeneration (Egger, Ladurner, Nimeth, Gschwentner, & Rieger, 2006; Lengerer et al., 2018), stem cell biology (Grudniewska

Jeremias N. Brand (jeremias.brand@unibas.ch); Pragya Singh (pragya.singh@unibas.ch); Kira S. Zadesenets (kira_z@bionet.nsc.ru); Claus-Peter Stelzer (claus-peter.stelzer@uibk.ac.at); Gudrun Viktorin (gudrun.viktorin@unibas.ch)

TABLE 1 Specimens analyzed for five *Macrostomum* species, *M. lignano* (Maclig), *M. janickei* n. sp. (Macjan), *M. cliftonensis* n. sp. (Maccli), *M. mirumnovem* n. sp. (Macmir), and *M. hystrix* (Machtx)

Species	Location	Origin	ID/worms	*28S* sequence	reads	*COI* sequence	Whole mount
Maclig	Lignano	LS1 (1)	MTP LS 244	FJ715326 (2)	–	KP730568 (3)	–
			6	–	3	MK690037	–
				–	3	MK690041	–
		DV1 (4)	2	–	2	MK690040	–
		DV4 (4)	2	–	2	MK690043	–
		DV6 (4)	2	–	2	MK690033	–
		DV16 (4)	2	–	2	MK690039	–
		DV18 (4)	2	–	2	MK690047 (a)	–
		DV22 (4)	2	–	2	MK690044 (a)	–
		DV47 (4)	2	–	2	MK690042	–
	Sithonia	LS3 (5)	MTP LS 2426	MK684173	–	–	–
			MTP LS 2427	MK684174	–	–	–
			MTP LS 2429	MK684175	–	–	–
			24	–	13 (6)	MK690035	–
				–	7 (7)	MK690034	–
Macjan	Palavas-les-Flots	B14 (8)	MTP LS 536	–	–	–	NMB-RHAB 00085b
			MTP LS 537	MK684168	2	MK690018	NMB-RHAB 00085a
		A1 (5)	Karyo 1	–	–	–	–
			Karyo 18	–	–	–	–
		Culture (5)	MTP LS 3212	MK684169	–	–	–
			4	–	4	MK690038	–
Maccli (9)	Lake Clifton	G7 (10)	**MTP LS 2896**	MK684170 (b)	2	MK690022	WAM V9393
			MTP LS 2906	same as (b)	2	MK690023	–
			MTP LS 2907	same as (b)	2	MK690031	WAM V9398
			MTP LS 2908	same as (b)	2	MK690029	WAM V9399
			MTP LS 2909	MK684171 (c)	2	MK690032	WAM V9400
			MTP LS 2910	–	–	–	–
			MTP LS 2911	same as (c)	0	–	–
			MTP LS 2931	same as (b)	2	MK690024	–
		G8 (11)	MTP LS 2901	same as (b)	2	MK690045	–
			MTP LS 2920	same as (c)	2	MK690030	WAM V9404
		G9 (12)	MTP LS 2903	same as (b)	2	MK690036	–
			MTP LS 2945	(13)	2	MK690021	WAM V9409
		G11 (14)	MTP LS 2900	same as (c)	2	MK690046	WAM V9396
			MTP LS 2930	same as (b)	0	–	–
Macmir (15)	Port Phillip Bay	A8 (16)	MTP LS 2993	–	–	–	NMW F258455
			MTP LS 2994	MK684172 (d)	2	MK690019	–
			MTP LS 2995	–	–	–	NMW F258456
			MTP LS 2996	–	–	–	–
		A13 (16)	MTP LS 3012	–	–	–	NMW F258461
			MTP LS 3014	–	–	–	NMW F258462
			MTP LS 3015	–	–	–	–
			MTP LS 3016	–	–	–	–
		C21 (17)	MTP LS 3019	same as (d)	2	MK690026	–
		D19 (17)	MTP LS 3147	same as (d)	2	MK690027	NMW F258509
		F11 (18)	MTP LS 3168	same as (d)	2	MK690025	NMW F258524
		E6 (19)	MTP LS 3498	same as (d)	2	MK690028	–

(Continues)

TABLE 1 (Continued)

Species	Location	Origin	ID/worms	*28S* sequence	reads	*COI* sequence	Whole mount
M. sp.	Lake Charra	–	MCZ DNA106151	KC869843 (20)	–	–	–
Machtx	Bibione	C12-14 (2)	MTP LS 68	FJ715323 (2)	–	KP730561 (3)	–
	San Rossore	SR1 (21)	MTP LS T8	–	2	MK690020	–

Notes: The table lists short species name, collection location, the laboratory culture or field sample that the worms originate from, specimen ID (bold if HOLOTYPE) or number of worms analyzed from laboratory cultures, GenBank accession number of partial *28S rRNA* gene sequences, the number of reads contributing to the *COI* gene sequence, GenBank accession number of partial *COI* gene sequences, and museum accession number of the stylet whole-mount permanent preparations (NMB, Natural History Museum Basel; WAM, Western Australian Museum; and NMW, Museum Victoria). Note that some specimens were not sequenced and that identical sequences of the same species are marked by the same bracketed letters and represented by the underlined specimen in the molecular analysis. Also note that the bracketed numbers refer to the footnotes. All newly deposited specimens are available on Zenodo at https://zenodo.org/record/2602479.
(1) Marie-Orleach et al. (2013).
(2) Schärer et al. (2011); specimens also available on Zenodo at https://zenodo.org/record/2581116.
(3) Janssen et al. (2015); specimens also available on Zenodo at https://zenodo.org/record/2580820; note that the originally deposited sequence KP730561 has now been corrected (https://www.ncbi.nlm.nih.gov/nuccore/KP730561.2), that is, the previously inserted N at the site of the frameshift deletion has been removed, based on the results presented here.
(4) Vellnow et al. (2017).
(5) Zadesenets et al. (2016).
(6) Two sequences differ in one base each (with both being silent third site mutations).
(7) Two sequences differ in one base each (with both being silent third site mutations).
(8) **Type locality:** sample B14 collected on 17 January 2009 from moist sand in the upper intertidal of a sheltered beach of a brackish water lagoon (at 10‰ salinity) near Palavas-les-Flots, France (N 43.50079, E 3.87226).
(9) PCR with adapted primers and sequencing with M13 primers; see also Table S1.
(10) **Type locality:** sample G7 collected on 17 January 2017 from sandy shore with reduced salinity water (35‰) seeping into a puddle on the shores of the increasingly hypersaline Lake Clifton (97‰ at time of sampling), Western Australia (S 32.76125, E 115.66019).
(11) Sample G8 collected on 17 January 2017 from sandy substrate with reduced salinity water (32‰) seeping out next to vegetation close to the type locality (S 32.76127, E115.66033)
(12) Sample G9 collected on 17 January 2017 from sandy substrate with reduced salinity water (65‰) seeping out next to vegetation close to the type locality (S 32.76111, E 115.66028)
(13) This sequence was not considered for analysis because it has ambiguities at the polymorphic sites
(14) Sample G11 collected on 17 January 2017 from sandy substrate with reduced salinity water (23‰) seeping out in between vegetation close to the type locality (S 32.76063, E 115.66037)
(15) PCR with adapted primers and sequencing with M13 primers; see also Table S1.
(16) **Type locality:** sample A1 collected on 28 January 2017 from the upper intertidal on a sheltered beach (at 35‰ salinity) in front of the Victorian Marine Science Consortium, Queenscliff, Port Phillip Bay, Victoria (S 38.27007, E 144.63894), and sample A13 collected from same site on 29 January 2017.
(17) Sample C21 collected on 30 January 2017 and sample D19 collected on 1 February 2017 from the upper intertidal under vegetation on a sheltered beach (at 35‰ salinity) in Edwards Point Wildlife Reserve, Port Phillip Bay, Victoria (S 38.21880, E 144.70047).
(18) Sample F11 collected on 8 February 2017 from the upper intertidal on a sheltered and drying pond (at 47‰ salinity) on Mud Island, Port Phillip Bay, Victoria (S 38.26964, E 144.76346).
(19) From a laboratory culture established from specimens collected in sample E6 on 6 February 2017 from a drainage ditch of Swan Bay Salt marsh, Queenscliff, Victoria (S 38.26503, E 144.62098).
(20) Laumer & Giribet, (2014).
(21) Ramm et al. (2015), Zadesenets et al. (2016).

et al., 2016; Ladurner et al., 2008), and sexual selection (Marie-Orleach, Janicke, Vizoso, David, & Schärer, 2016; Schärer, Littlewood, Waeschenbach, Yoshida, & Vizoso, 2011; Sekii et al., 2013). This research has led to the establishment of many resources and tools that are crucial for a modern genetic and genomic model, including in situ hybridization (Pfister et al., 2008), RNA interference (Kuales et al., 2011; Sekii et al., 2013), gene expression (Arbore et al., 2015; Grudniewska et al., 2016; Lengerer et al., 2018), genome and transcriptome assemblies (Wasik et al., 2015; Wudarski et al., 2017), transgenesis (Marie-Orleach, Janicke, Vizoso, Eichmann, & Schärer, 2014; Wudarski et al., 2017), and a clarification of the phylogenetic context (Janssen et al., 2015; Schärer et al., 2011). Jointly, these achievements make *M. lignano* an excellent model to complement the, in several aspects, more established planarian flatworm models (Newmark & Sánchez Alvarado, 2002; Pellettieri & Sánchez Alvarado, 2007; Rink, 2013; Rouhana et al., 2013). This is in part linked to the high transparency of *Macrostomum* flatworms, which is particularly powerful in combination with transgenesis tools (Marie-Orleach et al., 2016; Wudarski et al., 2017), which so far have proven difficult to establish in planarian flatworms, possibly due to their unusual embryology (Cardona, Hartenstein, & Romero, 2005).

In spite of its general appeal as a flatworm model, the further establishment of *M. lignano* as a broadly employed genetic and genomic model has recently run into a roadblock. Such models should ideally have small and stable genomes, facilitating the establishment of (a) highly contiguous genome assemblies, (b)

high-resolution genetic maps for forward genetics using quantitative trait loci (QTL) and genome-wide association studies (GWAS; Bazakos, Hanemian, Trontin, Jiménez-Gómez, & Loudet, 2017), and (c) efficient genome editing for reverse genetics (e.g., CRISPR/Cas9; Brooks & Gaj, 2018). In this light, the recent discovery that *M. lignano* has an unusual genome organization is problematic. Earlier work had suggested that *M. lignano* has a 2n = 8 karyotype (with two large and six small chromosomes), while most other *Macrostomum* species are 2n = 6 (with six small chromosomes), or more rarely 2n = 12 (with twelve small chromosomes) (Egger & Ishida, 2005). Subsequent karyological analyses have confirmed this unusual karyotype and also revealed that individual *M. lignano* can deviate from the 2n = 8 karyotype and that such variation segregates within freshly field-collected worms, outbred laboratory cultures, and also inbred lines (Zadesenets et al., 2016). Most of this variation involves the presence of either 2, 3, or 4 copies of the large chromosome (yielding 2n = 8, 2n = 9, and 2n = 10 individuals, respectively), but individuals with additional karyotypes (including some with chromosomal rearrangements) also occur at low frequency (Zadesenets et al., 2016). More recent analyses have further shown that the large chromosome represents a fusion product of one full haploid chromosome set, making the 2n = 8, 2n = 9, and 2n = 10 karyotypes effectively hidden tetra-, penta-, and hexaploids, respectively. It is likely that this situation emerged from a recent whole-genome duplication that was followed by a rediploidization into a 2n = 8 karyotype (Zadesenets, Ershov, Berezikov, & Rubtsov, 2017a; Zadesenets, Schärer, & Rubtsov, 2017b). These recent insights—and the complex genome organization they reveal—clearly dampen the prospects of *M. lignano* becoming a full-fledged genetic and genomic model.

Here, we present efforts to find alternatives within the species-rich *Macrostomum* genus, which could supplement or even replace *M. lignano* as the primary model. We have collected several new and currently undescribed *Macrostomum* species, which—as we show below—are closely related to *M. lignano*. The new species include *Macrostomum janickei* Schärer n. sp., *Macrostomum cliftonensis* Schärer and Brand n. sp., and *Macrostomum mirumnovem* Schärer and Brand n. sp. We describe these species taxonomically, covering both anatomical and behavioral aspects, place them phylogenetically using molecular analyses, and—by determining their karyotypes and genome sizes—evaluate their suitability as genetic and genomic models.

2 | MATERIALS AND METHODS

2.1 | Collection, documentation, preservation, and specimen deposition

Details on species and specimens included are given in Table 1. Briefly, *M. lignano* was collected in the Northern Adriatic Sea (including the type locality) and the Aegean Sea (Ladurner et al., 2005; Zadesenets et al., 2016), and *M. janickei* was collected in the Gulf of Lion (Zadesenets et al., 2016; called *Macrostomum* sp. 8 therein). Long-term laboratory cultures have been established from these species, including genetically outbred cultures (of both *M. lignano* and *M. janickei*) and inbred lines (of *M. lignano*) (Vellnow, Vizoso, Viktorin, & Schärer, 2017; Zadesenets et al., 2016). Furthermore, we have collected *M. cliftonensis* from the shores of Lake Clifton, an increasingly hypersaline coastal lake South of Perth (Western Australia; Lane, Clarke, & Winchcombe, 2017), as well as *M. mirumnovem* from several sites in Port Philipp Bay near Queenscliff (Victoria). Long-term outbred laboratory cultures of both species have been established. As the outgroup for the molecular analyses (see below) we use *Macrostomum hystrix* Ørsted 1843, collected from two locations in Italy, a species previously shown to be genetically close to *M. lignano* (Schärer et al., 2011).

Specimens were either collected directly from the field or taken from laboratory cultures, and many specimens were extensively documented morphologically using digital photomicrography; when possible, we also prepared whole-mount permanent preparations of the stylet, the male intromittent organ (see Janssen et al., 2015; Schärer et al., 2011). Whole worms or fragments were then preserved in either absolute ethanol (stored cool for at most a few weeks and then at −20°C) or RNAlater (stored at 4°C for at most a few weeks and then at −80°C). The studied specimens were then deposited on the Macrostomorpha Taxonomy and Phylogeny website (at http://macrostomorpha.info), the images and videos were deposited in the open access repository Zenodo (at https://doi.org/10.5281/zenodo.2602479), and the whole-mount permanent preparations were deposited in various museums (Table 1).

2.2 | Image processing

The images used in the species description panels were processed in Photoshop (version 2017.1.1), including rotation and cropping from the original digital images (filling in blank spaces with the approximate background color), and contrast enhancement using the "Levels" function. Moreover, overview images were stitched manually (including slight adjustments of the aspect ratios to compensate for worm movement) or using the "Photomerge" function (using the reposition function), and these are labeled "stitched" in the panels. Finally, some structures are visualized using the "Auto-Blend Layers" function, where different focal planes (in our case a video focusing through the structure of interest) are synthesized into a single compound image, and these are labeled "merged" in the panels. While such images facilitate visualization of structures in different focal planes, they can be somewhat misleading in that they can hide curvature in the *z*-axis.

2.3 | Morphometrics

Morphometric analyses (see Table 2) were performed using the software ImageJ (version 1.51w) and the plugin ObjectJ (version 1.04r), which allows marking structures in the original images in a non-destructive manner. The pixel length of structures was converted into µm by calibration using a stage micrometer. Body length was measured by placing a segmented line along the central body axis. Body width was measured by placing a line perpendicular to the body axis

at the height of the testes. Testis and ovary lengths were measured as the longest distance of the structure parallel to the body axis. Eye diameter, sensory cilia length, rhabdite granule length, straight stylet length, the width of the stylet openings, sperm bristle length, and sperm brush length were measured by placing a straight line along the structures. To measure segmented stylet length, we placed a segmented line along both sides of the stylet and averaged the length. For sperm length, we placed a segmented line along the central axis of the sperm. We defined sperm feeler length and sperm body length as previously described (Janicke & Schärer, 2010).

2.4 | Mating behavior

We analyzed mating behavior using established techniques (Marie-Orleach, Janicke, & Schärer, 2013; Schärer, Joss, & Sandner, 2004). Briefly, worms were paired and placed in small drops between two glass slides with spacers, then filmed in the resulting mating chamber using time-lapse video (1 frame per second), and behaviors scored from the resulting video sequences. Here, we present only a brief characterization of the behaviors of these species based on a single mating pair and compare these observations to the behaviors observed in *M. lignano* (Schärer et al., 2004). Briefly, *M. lignano* shows a reciprocal mating behavior, where partners first reciprocally engage in a precopulatory behavior called *circling*, during which the worms crawl around on each other. This then often leads to a characteristic copulatory posture that resembles two interlocking "G" characters forming a tight disk, during which the worms reciprocally insert their stylet into the partner's female antrum via the female gonopore and during which the anterior ventral surface of each worm is in contact with the partner's posterior dorsal surface. Copulations on average last for 8.8 s (range: 5–16 s). Once the copulation ends, the worms often show a stereotypical behavior called *sucking*, during which a worm places its mouth opening over its own female gonopore, presumably in an attempt to remove ejaculate components from the female antrum (Schärer et al., 2004, 2011). This *sucking* behavior on average lasts 4.9 s (range: 4–7 s) and is performed, generally within 5 s, by either none, one, or both worms after about a third of the copulations, respectively.

The paired *M. janickei* adults were isolated as hatchlings from the laboratory culture (and were thus virgins), the paired *M. cliftonensis* were field-collected worms from the type locality, and the paired *M. mirumnovem* were isolated for over a week after being taken from the laboratory culture (isolating worms prior to pairing can increase the likelihood of observing matings). More detailed analyses of the mating behaviors of the new species are underway (P. Singh, D. Ballmer, M. Laubscher, & L. Schärer, unpublished data).

2.5 | Karyology and genome size

Metaphase plates were prepared from individual worms of *M. janickei*, *M. cliftonensis*, *M. mirumnovem*, and *M. hystrix*, using the single-worm karyotyping technique described previously (Zadesenets et al., 2016). Chromosomes were counterstained with VECTASHIELD Antifade Mounting Medium with DAPI (Vector Laboratories). Specimens of *M. janickei* were taken from natural populations, while specimens of *M. cliftonensis*, *M. mirumnovem*, and *M. hystrix* were taken from outbred laboratory cultures (Table 1). In total, we always analyzed ≥10 metaphase spreads per individual. Microscopic analysis of chromosome slides was done using a CCD-camera installed on an Axioplan 2 compound microscope (Carl Zeiss) equipped with filter cube #49 (ZEISS) using ISIS4 software (MetaSystems GmbH) at the Inter-institutional Shared Center for Microscopic Analysis of Biological Objects (Institute of Cytology and Genetics SB RAS).

To obtain genome size estimates from the studied *Macrostomum* species, we used a detergent–trypsin method with propidium iodide (PI) staining for flow cytometric analysis of genome size (Stelzer, Riss, & Stadler, 2011). Briefly, for each replicate 7–20 starved worms were washed in few mL of stock solution (3.4 mM Trisodium citrate dihydrate, Nonidet P-40 at 0.1% v/v, 1.5 mM Spermine tetrahydrochloride, 0.5 mM Tris(hydroxymethyl)-aminomethane, pH 7.6) and then transferred to 750 µl of stock solution in a 1 ml Dounce tissue homogenizer. Worms were homogenized on ice with 20 strokes using the "tight" pestle of the homogenizer. As an internal standard of known genome size, we used the fruit fly, *Drosophila melanogaster* (strain ISO-1, diploid nuclear DNA content: 0.35 pg; Gregory, 2019). After adding two female *Drosophila* heads, the sample was further homogenized with ten strokes. Large debris was removed by filtration through a 40 µm mesh nylon sieve. After addition of 100 µl of 0.021% Trypsin (dissolved in stock solution), the sample was incubated for exactly 10 min at 37°C. To prevent further degradation, 75 µl of 0.25% trypsin inhibitor was added (this solution also included 0.05% RNase A) and the samples were incubated for another 10 min at 37°C. Finally, samples were stained with propidium iodide at a concentration of 50µg/ml and kept overnight on ice in the dark. Flow cytometric analysis was performed on the next day on an Attune NxT acoustic focusing cytometer (ThermoFisher) with an excitation wavelength of 561 nm (yellow) and a custom-made 590–650 nm bandpass filter for detection of PI fluorescence. Flow cytometric data were analyzed using FlowJo software version 10.0.7r2 (FlowJo LLC). Flow cytometry events were gated by YL2A versus YL2H for doublet exclusion. Coefficients of variance (CVs) of individual peaks typically ranged between 1.5% and 6% for both *Drosophila* and worms. Very few measurements had CVs higher than 6%, and those replicates were discarded. Conversion from picograms DNA to base pairs were made with the factor: 1 pg = 978 Mbp (Gregory, 2019).

2.6 | Molecular phylogenetic placement

To determine the molecular phylogenetic placement, we initially used a partial (nuclear) *28S ribosomal RNA* (*28S rRNA*) gene sequence, a marker previously used in *Macrostomum* (Schärer et al., 2011). However, as outlined below, this marker was too conserved to successfully resolve interrelationships between *M. lignano* and *M. janickei*. We therefore also used a partial (mitochondrial) *cytochrome c oxidase I* (*COI*) gene sequence, a more rapidly evolving marker

TABLE 2 Morphometric measurements based on image and video material from the deposited specimens of the three new *Macrostomum* species, *M. janickei* n. sp., *M. cliftonensis* n. sp. and *M. mirumnovem* n. sp.; L: length, W: width

	M. janickei n. sp.				*M. cliftonensis* n. sp.				*M. mirumnovem* n. sp.			
Parameter	**Mean (µm)**	***SD* (µm)**	**range (µm)**	***n***	**Mean (µm)**	***SD* (µm)**	**range (µm)**	***n***	**Mean (µm)**	***SD* (µm)**	**range (µm)**	***n***
Body L	1,153	430	701–1731	4	1,220	312	709–1762	14	1,170	333	670–1667	12
Body W	339	151	143–496	4	324	81	214–456	14	329	94.6	169–441	12
Eye ø	8.3	1.9	6.9–9.6	2	10.1	1.7	7.2–12.6	11	9.2	1.2	7.2–10.1	5
Testis L	224	8.7	217–230	2	221	50.8	167–328	13	64.8	16.1	40.3–94.1	11
Ovary L	126	64.2	80.8–172	2	120	46.6	58.3–221	12	140	51.9	73.6–227	9
Short sensory cilia L	10.2	1.7	8.8–12.2	3	10	1.4	7.3–12.3	8	7.5	1.9	4.4–9.3	6
Long sensory cilia L	14.6	-	-	1	26	8.6	15.4–40.7	7	11.2	0.4	11–11.6	3
Rhabdite L	7.2	2.1	4.8–9.4	4	6.9	1.2	5.3–10.1	12	6.1	0.4	5.2–6.6	10
Stylet traits												
Straight L	72	5.9	67.8–76.2	2	123	10.7	98.5–132	10	83.3	9.6	60.4–93.4	9
Segmented L	69.1	10.3	57.5–77.0	3	126	8.5	111–140	11	89.8	7.2	78–101	10
Proximal opening W	21.9	8.3	13.9–30.5	3	19.4	4.7	13.9–30	11	13.3	2.7	10.4–19.9	10
Distal opening W	6.1	1.9	4.9–8.4	3	7.9	2.2	3.9–11.5	11	4.1	1.4	1.8–6.6	9
Sperm traits												
Total L	81.1	2.1	79.6–82.6	2	103	2.8	98.1–106	5	86	5.8	79.9–92.5	6
Feeler L	22.7	5.7	18.7–26.8	2	24.4	3	20.1–28.1	5	32.5	5.7	26.2–41	5
Body L	11.6	4.1	8.7–14.5	2	14.5	0.8	13.8–15.6	5	13	1.1	11.1–14.2	5
Bristle L	13.6	0.9	13–14.3	2	12.3	0.5	11.8–12.8	5	11.5	0.6	10.5–12.2	6
Brush L	4.8	0.2	4.6–4.9	2	3.8	0.4	3.3–4.1	4	3.4	1.2	2.1–4.6	5

previously used in the Macrostomorpha (Janssen et al., 2015). Moreover, to better understand the intraspecific phylogenetic structure, we sequenced the partial *COI* gene in multiple specimens per species, including several *M. lignano* laboratory lines and cultures, as well as field-collected specimens. As an outgroup, we used *M. hystrix*, a species that is closely related to *M. lignano* (Schärer et al., 2011).

DNA was extracted either, for worms stored in ethanol, using the DNeasy Blood and Tissue kit (Qiagen, Germany) following evaporation of ethanol, or, for worms stored in RNAlater, using the NucleoSpin RNA XS kit with the combined RNA/DNA buffer set (Macherey-Nagel, Germany). Extracted DNA samples were stored at −80°C until used.

We used the ZX-1 and 1500R primers to amplify the partial *28S rRNA* gene sequence (Table S1; Schärer et al., 2011), yielding PCR fragments of 1,177 bp (with respect to the *M. lignano* sequence) and Sanger sequenced the resulting fragments in both directions using the same primers (Microsynth, Switzerland) (and in one case additional internal sequencing primers, 300F and ECD2; Schärer et al., 2011). Cycling conditions were either as in Schärer et al. (2011), or using Q5 Hot Start polymerase (NEB), 98°C for 30 s, 7 touchdown cycles with denaturation for 7 s at 98°C, annealing for 30 s with temperatures starting at 70°C and decreasing 1°C each cycle, elongation at 72°C for 20 s, followed by 28 more cycles with 64°C annealing temperature and a final elongation for 2 min at 72°C. All reads were subjected to BLAST searches (http://www.ncbi.nlm.nih.gov) to check for possible contaminations, then de novo assembled into consensus sequences in Geneious (11.1.4, Biomatters) using the built-in assembler (with the highest sensitivity). The resulting assemblies were visually checked, manually trimmed and edited where necessary. For all in-group species, multiple specimens were sequenced and one representative specimen was chosen for each unique consensus sequence (Table 1). The resulting sequences were aligned in Geneious using MAFFT (v7.388), with default settings (using FFT-NS-i x1000). The alignment was trimmed to a uniform length of 1,040 bp (see Alignment S1), and then, a consensus tree was generated using Geneious Tree Builder (using Tamura-Nei Neighbor Joining, with 1,000 bootstrap samples), and *M. hystrix* was used to root the tree. As outlined below, the tree topology suggested that this partial *28S rRNA* gene sequence is not variable enough to resolve the interrelationships between *M. lignano* and *M. janickei*. More elaborate analyses were therefore not considered and effort instead focused on the *COI* gene, which we describe next.

We used a range of primers to amplify the partial *COI* gene (Table S1). Unless otherwise stated, we used Mac_COIF and Mac_COIR (Janssen et al., 2015), optimized using a *M. lignano* mitochondrial genome (NCBI Reference Sequence: NC_035255.1; Egger, Bachmann, & Fromm, 2017), yielding a PCR fragment of 709 bp. Alternatively, we used PCR primers optimized using whole-body transcriptome data of *M. cliftonensis* and *M. mirumnovem* (Brand et al., unpublished data), respectively, yielding PCR fragments of 1,125 bp (excluding the M13 tails). Cycling conditions for these primers were analogous to the *28S rRNA* gene, except a duration of 40 s was used for all elongations. Moreover, we either used 7 touchdown cycles with annealing temperatures decreasing from 70 to 59°C, followed by 28 cycles using 59°C as annealing temperature, giving a total of 35 cycles. Or we used 11 touchdown cycles with 2 min annealing time and annealing temperatures decreasing from 68 to 56°C followed by nine cycles with annealing for 1 min at 56°C and 20 cycles with annealing for 30 s at 64°C, giving a total of 40 cycles. The resulting fragments were generally Sanger sequenced in both directions using the PCR primers (or using the M13 tails of the primers for *M. cliftonensis* and *M. mirumnovem*). For the Mac_COIF/Mac_COIR primers, the quality of the resulting sequences was somewhat variable, particularly for the reverse primer. For these sequences, we therefore, in some cases, decided to de novo assemble multiple specimens, which in most cases yielded well-supported consensus sequences (Table 1). Note that the different DV lines of *M. lignano* represent inbred lines initiated from a single mother, which are therefore expected to have just one mitochondrial cytotype within each line (see also Vellnow et al., 2017), which was also confirmed by our *COI* gene sequences.

For alignment, these protein-coding sequences were translated with the echinoderm and flatworm mitochondrial code (transl_table = 9; Telford, Herniou, Russell, & Littlewood, 2000), using the reading frame of the annotated *COI* gene in the *M. lignano* mitochondrial genome (Egger et al., 2017). This revealed that both of the analyzed *M. hystrix* specimens showed a single-base deletion at position 336 (counting from the ATT start codon of the 1,548 bp *COI* gene), leading to a frameshift mutation and a TAG stop codon only 10 bases on (and 8 more stop codons in the sequenced fragment alone), which one would expect to lead to truncation the resulting COI protein. Given the importance of the COI protein in the electron transport chain of mitochondrial oxidative phosphorylation, this finding was surprising and required further validation (see Section 3).

For phylogenetic analysis, we inserted an "N" character in place of the deletion, as was also done for the originally deposited *COI* gene sequence of *M. hystrix* (KP730561 in Janssen et al., 2015), so that the alignment, which was trimmed to a uniform length of 573 bp (Alignment S2), generated a correct protein-coding sequence in all specimens. From this alignment, a maximum likelihood tree was calculated with IQ-TREE (multicore version 1.6.10; Nguyen, Schmidt, Haeseler, & Minh, 2015). We first ran ModelFinder (Kalyaanamoorthy, Minh, Wong, von Haeseler, & Jermiin, L. S., 2017), which identified HKY + F + G4 as the best fitting substitution model (BIC = 4,906.3), and we then ran a tree reconstruction with 500 non-parametric bootstrap replicates.

2.7 | Nomenclatural acts

The electronic edition of this article conforms to the requirements of the amended International Code of Zoological Nomenclature (ICZN), and hence, the new names contained herein are available under that code from the electronic 'Early View' edition of this article (published in 2019).

This published work and the nomenclatural acts it contains have been registered in ZooBank, the online registration system for the ICZN. The ZooBank LSIDs (Life Science Identifiers) can be resolved and the associated information viewed through any standard web browser by appending the LSID to the prefix "http://zoobank.org/". The LSID for this publication is: urn:lsid:zoobank.org:pub:4CDD54C7-B44E-4070-8D8F-92C170C3EF4E. The journal's Online ISSN is 1439-0469 and it is archived in CLOCKSS. Note that these names have also appeared in the electronic 'Early View' edition of another article from our group (Singh, Vellnow, & Schärer, 2019), but since that work was not intended to conform to the ICZN requirements, having an experimental rather than taxonomic focus, these names cannot be considered available from that work.

3 | RESULTS AND DISCUSSION

Species descriptions

Family Macrostomidae Van Beneden, 1870

Genus *Macrostomum* Schmidt, 1848

Macrostomum janickei Schärer, n. sp.

urn:lsid:zoobank.org:act:56A75401-E27A-4814-8176-B34F5CC3B714 (Figures 1–3; Figure 10a, b; Figure 11a, b; Table 1, Table 2)

Material examined. Live observations on four field-collected specimens and several specimens from laboratory cultures. Holotype:

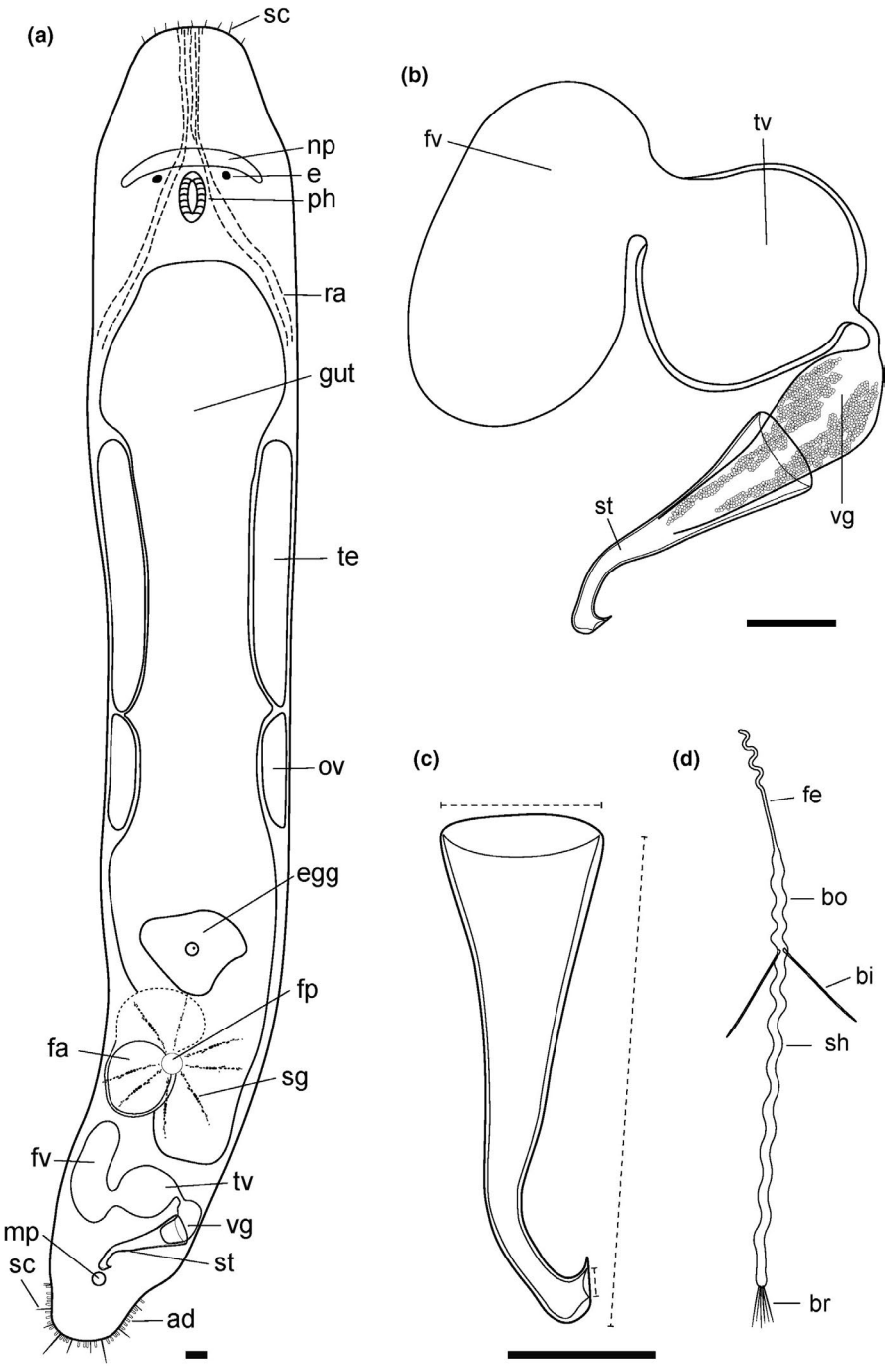

FIGURE 1 Line drawings of *Macrostomum janickei* n. sp.: (a) Habitus (viewed from dorsal and lightly squeezed), with sensory cilia (sc), neuropile (np), eyes (e), pharynx (ph), rhammites (ra), testis (te), ovary (ov), female gonopore (fp), female antrum (fa), shell glands (sg), male gonopore (mp), and adhesive glands (ad). (b) Male genital system with (non-muscular) false seminal vesicle (fv), muscular true seminal vesicle (tv), vesicula granulorum (vg), and stylet (st). (c) Detailed drawing of the stylet (indicated are the measurements for the straight stylet length and the width of the proximal and distal stylet openings, while the segmented stylet length corresponds to the average length of both sides of the stylet). (d) Mature sperm cell with feeler (fe), body (bo), bristles (bi), shaft (sh), and brush (br)

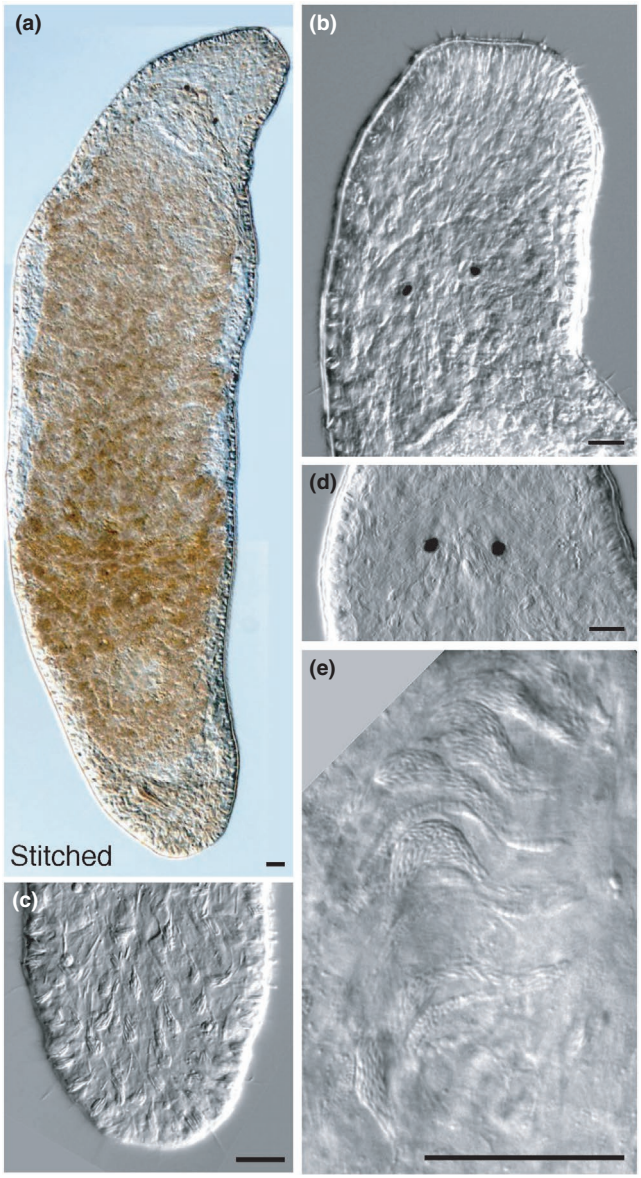

FIGURE 2 Micrographs of somatic structures of *Macrostomum janickei* n. sp. collected from the field (the bracket denotes the code of the deposited specimen, with MTP LS 537 being the HOLOTYPE; note that all specimens, except Karyo 18, were imaged from the dorsal side). (a) Overview of an adult, lightly squeezed, worm (Karyo 18, manually stitched from 3 images); (b) head region with neuropile, eyes, and pharynx; note the short sensory hairs on the rostrum (MTP LS 537); (c) tail region with dense rhabdite bundles and several long sensory hairs (MTP LS 537); (d) eyes with rhammite gland secretions penetrating the neuropile (MTP LS 536); (e) details of the pharynx gland necks showing two distinct pharyngeal gland secretions (MTP LS 537). Scale bars 25 μm

one extensively documented worm (MTP LS 537, 60 images and videos) from the type locality (i.e., sample B14 collected on 17 January 2009 from moist sand in the upper intertidal of a sheltered beach of a brackish water lagoon near Palavas-les-Flots, France; N 43.50079, E 3.87226), including a whole mount (NMB-RHAB 00085a) and a partial *28S rRNA* gene sequence. Paratypes: one extensively documented worm from same sample as holotype (MTP LS 536, 54 images and videos), including a whole mount (NMB-RHAB 00085b); two partly documented specimens (Karyo 1 and Karyo18; karyology failed, specimens not deposited), collected in 2014 from near the type locality; one worm from laboratory culture, established from the 2014 collections, extensively documented in 2017 (MTP LS 3212, 30 images and videos; see also Table 2); and 4 undocumented worms from laboratory culture for sequencing of the partial *COI* gene.

Etymology. Species name in honor of Tim Janicke, who was the first to culture this species during his PhD with LS, and who has assisted LS during multiple subsequent collections. To facilitate backwards compatibility with previous records and reports, note that this species has previously been referred to as *Macrostomum* sp. 8 (or Mac008 for short).

Diagnosis. *Macrostomum* with spindle-shaped body and trapezoid rostrum (Figure 1a; Figure 2a). Body lengths of field caught worms range from 701 to 1731 μm (see also Table 2). Sensory cilia are generally short and restricted to rostrum and tail plate. Two small pigment cup eyes. Gut extends caudally beyond female antrum. Testes clearly larger than ovaries. The highly distinctive stylet (~70 μm), is a long and gradually narrowing funnel that includes first a slight turn (of ~40°) and then a sharp turn (of >90°) toward the distal end (Figure 1c), leading to the distal opening being oriented laterally and obliquely cut off (Figure 1c), giving the stylet tip a hook-like appearance. Prostate granules of vesicula granulorum reach into about half the length of the stylet. The vagina is central and the female antrum—often containing received sperm—appears relatively complex and may be displaced slightly toward the left side of the body. Sperm (81 μm) show general morphology of reciprocally mating species (Schärer et al., 2011).

Description (see also Table 2)

General morphology. The body is spindle-shaped (width/length ratio: 1:3.4) and widest at the level of the anterior testes (Figure 1a; Figure 2a). The rostrum is trapezoid (Figure 2b), and the tail plate is relatively indistinct. The pigment cup eyes are small and fairly round (Figure 2d). The body is covered homogeneously with cilia, and sensory cilia are largely restricted to the rostrum and tail region, being very short and stiff on the rostrum and longer on the tail (Figure 2c). The mouth and pharynx are unremarkable (Figure 2e), and the gut extends posteriorly beyond the female antrum, ending at the seminal vesicles at 80% BL (% of body length). Rhabdite bundles are sparse, and most abundant on the dorsal side of the head and tail (Figure 2c), forming bundles of 6–12 granules. The rhammite glands originate dorsally anterior of the testes, and their granules are secreted via the neuropile into the anterior rostrum, where prominent rhammite bundles can be observed. The adhesive glands are arranged horseshoe-like in a single line along the edge of the tail plate.

Male system. The prominent testes extend from 27% to 40% BL and show developing sperm aligned in the center (Figure 3a). While the vas deferens is not easily seen, in some specimens one can see how the developing sperm appear to be aligned to enter the vas deferens, in a position where the distal side of the testis is in contact

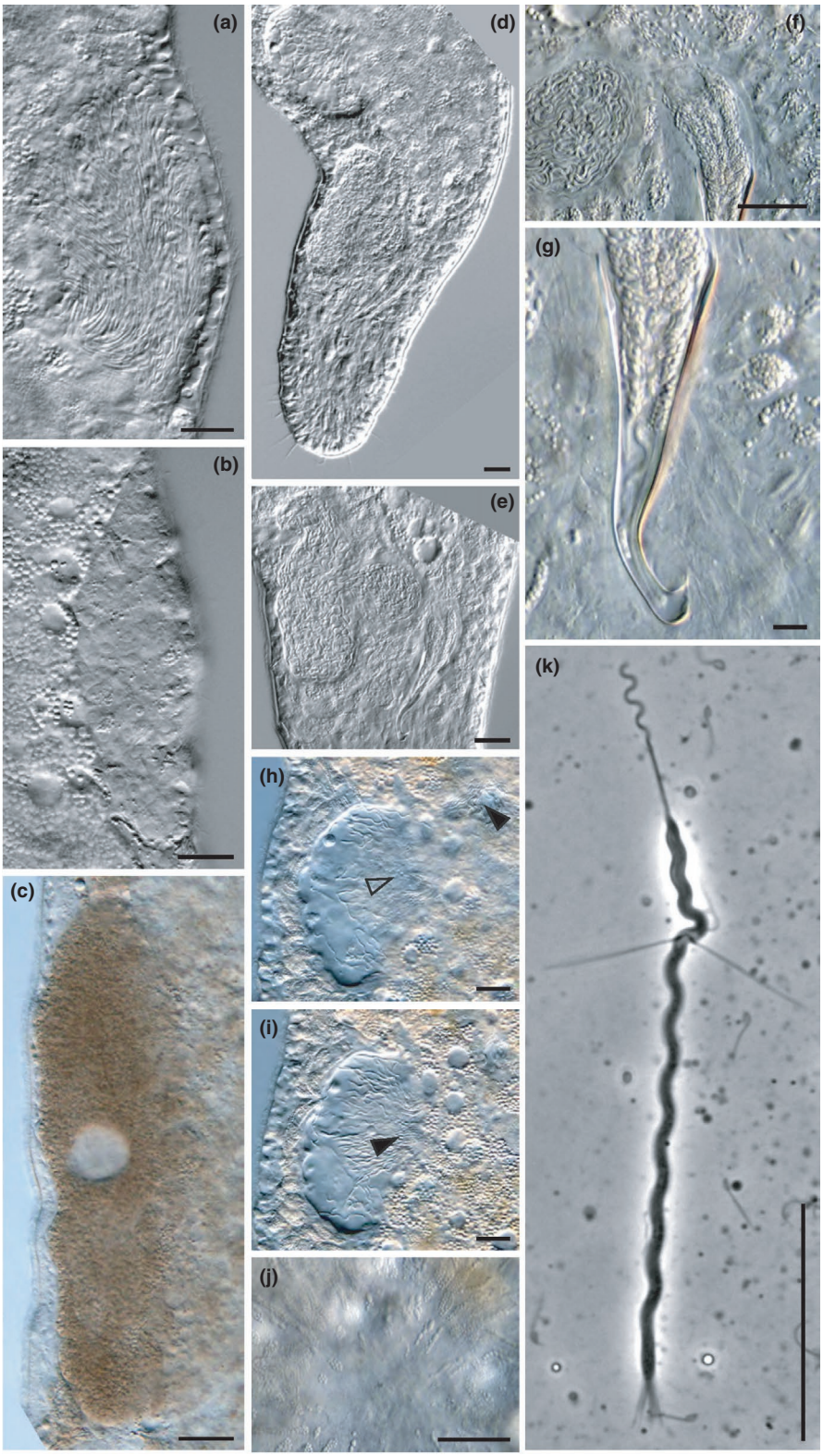

FIGURE 3 Micrographs of reproductive structures of *Macrostomum janickei* n. sp. collected from the field (the bracket denotes the code of the deposited specimen, with MTP LS 537 being the HOLOTYPE; note that all specimens, except MTP LS 2908, were imaged from the ventral side). (a) ripe testis with elongating spermatids aligned in the central region (MTP LS 536); (b) ripe ovary with oocytes that are beginning to form yolk and shell granules (MTP LS 537); (c) forming egg with the clearly visible nucleus, and many yolk and shell granules (Karyo 1); (d) body region containing the female antrum, the false and true seminal vesicle, vesicula granulorum, and stylet; note the long sensory hairs on the tail plate (MTP LS 537); (e) false and true seminal vesicle, vesicula granulorum, and stylet (MTP LS 537); (f) muscular true seminal vesicle, ductus intervesicularis, vesicula granulorum, and base of the stylet (MTP LS 537, frame extracted from a movie); (g) stylet showing the sharply turning distal end and prostate gland necks reaching far into the stylet (MTP LS 537, frame extracted from a movie); (h) female antrum with received sperm and coagulated seminal fluid; note the ciliary tuft near the center (open arrowhead) and the anchored bundle of sperm reaching the upper right corner (closed arrowhead) (MTP LS 537, frame extracted from a movie). (i) Female antrum with received sperm and coagulated seminal fluid; note the anchored bundle of sperm right of center (closed arrowhead) in the region of the ciliary tuft (MTP LS 537, frame extracted from a movie). (j) Vagina region surrounded by shell glands (MTP LS 537, frame extracted from a movie). (k) Sperm with typical feeler, body, bristles, shaft, and brush (MTP LS 536). Scale bars 25 μm

with the gut region. There is a prominent (non-muscular) false seminal vesicle that lies on the left of the tail plate (Figures 1b, 3d), connecting to a muscular true seminal vesicle that lies quite centrally (Figure 3e). The true seminal vesicle is connected via a short ductus intervesicularis to the prominent and muscular vesicula granulorum (Figure 3f) that sits on the proximal stylet opening. The tail plate contains many prostate gland cells that send out their necks into the vesicula granulorum, from which prostate glands necks reach to about half the length of the stylet (Figures 1b, 3g). The stylet is a gradually narrowing funnel that includes a slight turn of about 40° at about 80% of its length, then turning sharply by more than 90° in a knee-like fashion in the last 5% of its length (Figure 1c). The

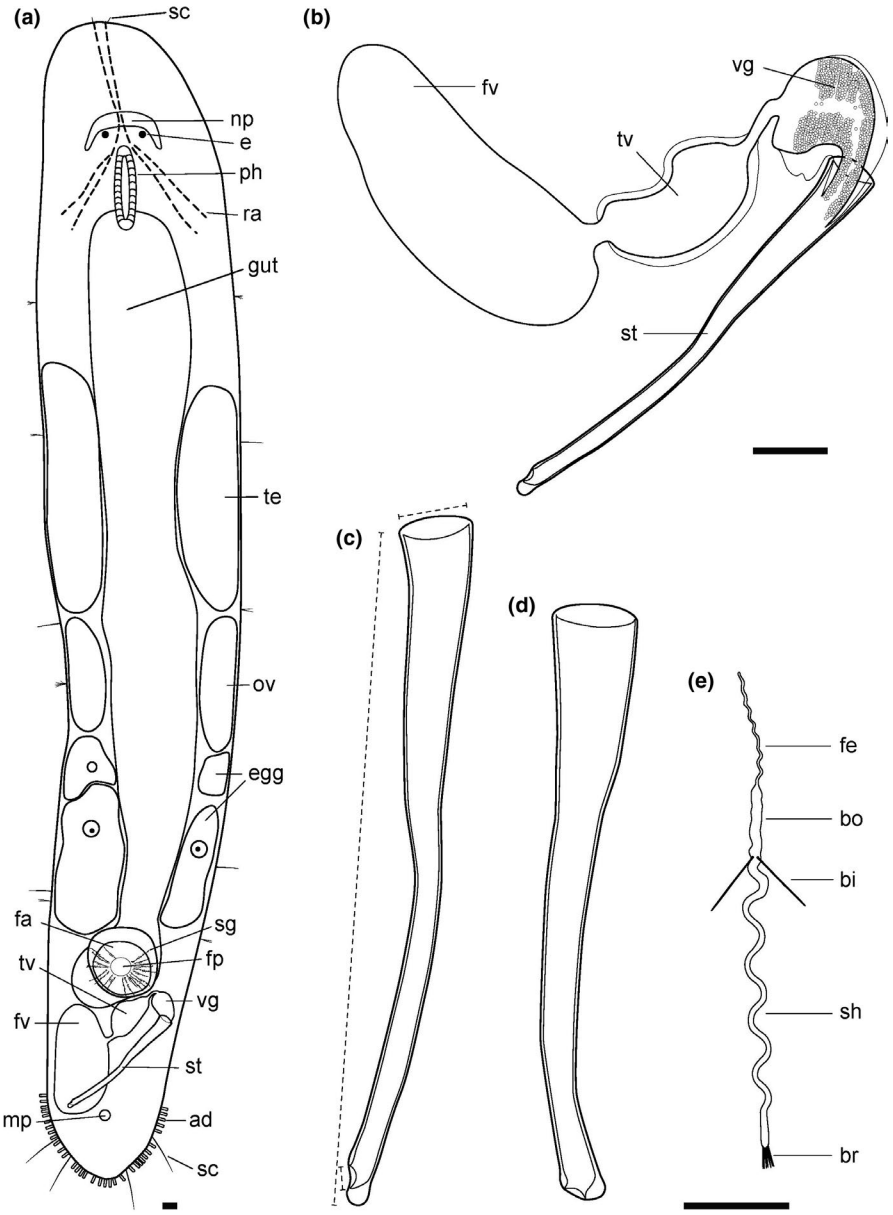

FIGURE 4 Line drawings of *Macrostomum cliftonensis* n. sp.: (a) Habitus (viewed from dorsal and lightly squeezed). (b) Male genital system with false seminal vesicle, muscular true seminal vesicle, vesicula granulorum, and stylet. (c) Detailed drawing of the most common view of the stylet. (d) Detailed drawing of an alternate view of the stylet (observed in MTP LS 2945). (e) Mature sperm cell with feeler, body, bristles, shaft, and brush (see Figure 1 for abbreviations)

outside turn of the knee is slightly thickened, while the inside turn ends in a point, leading to the distal opening being oriented laterally and being obliquely cut off (Figure 1c). Together, this gives the stylet a resemblance of a hook. The male canal ends in an unremarkable male antrum, and the male gonopore (at 95% BL) is slightly ciliated. The sperm (Figures 1d; 3k) have the usual morphology for a species in the reciprocally mating clade (Schärer et al., 2011).

Female system. The relatively small ovaries lie directly behind the testes, extending from 45% to 54% BL (Figures 1a, 3b). The developing eggs show ample yolk and shell granules (Figure 3c). Eggs in progressive stages of development propagate posterior from the ovaries and are frequently seen in the central body region before they enter the female antrum. The female antrum is relatively complex, and parts of it appear to be displaced somewhat to the left side of the body (Figures 1a, 3d, h–i), while the vagina appears to lie centrally (at 79% BL). Received sperm can often be observed in multiple locations, on the one hand opposite of the vagina (closed arrowhead in Figure 3i), but in many specimens also in more anterior regions (closed arrowhead in Figure 3h), which suggest that there may be a second chamber to the antrum, or a relatively loose cellular valve that sperm can penetrate deeply. Where the vagina enters the female antrum, there is a dense ciliary tuft with long cilia that reach into the antrum lumen (open arrowhead in Figure 3h). Relatively sparse shell glands surround the vagina extending to approximately the width of the animal (Figure 3j).

Mating behaviour. In Video S1, the worms engage in precopulatory behavior from 13 to 49 s, during which they circle while trying to get into the copulatory posture. The copulation starts at 50 s and ends at 147 s, lasting for ~97 s. During the copulation, the worms are interlinked in a disk-like posture and rotate intermittently about their

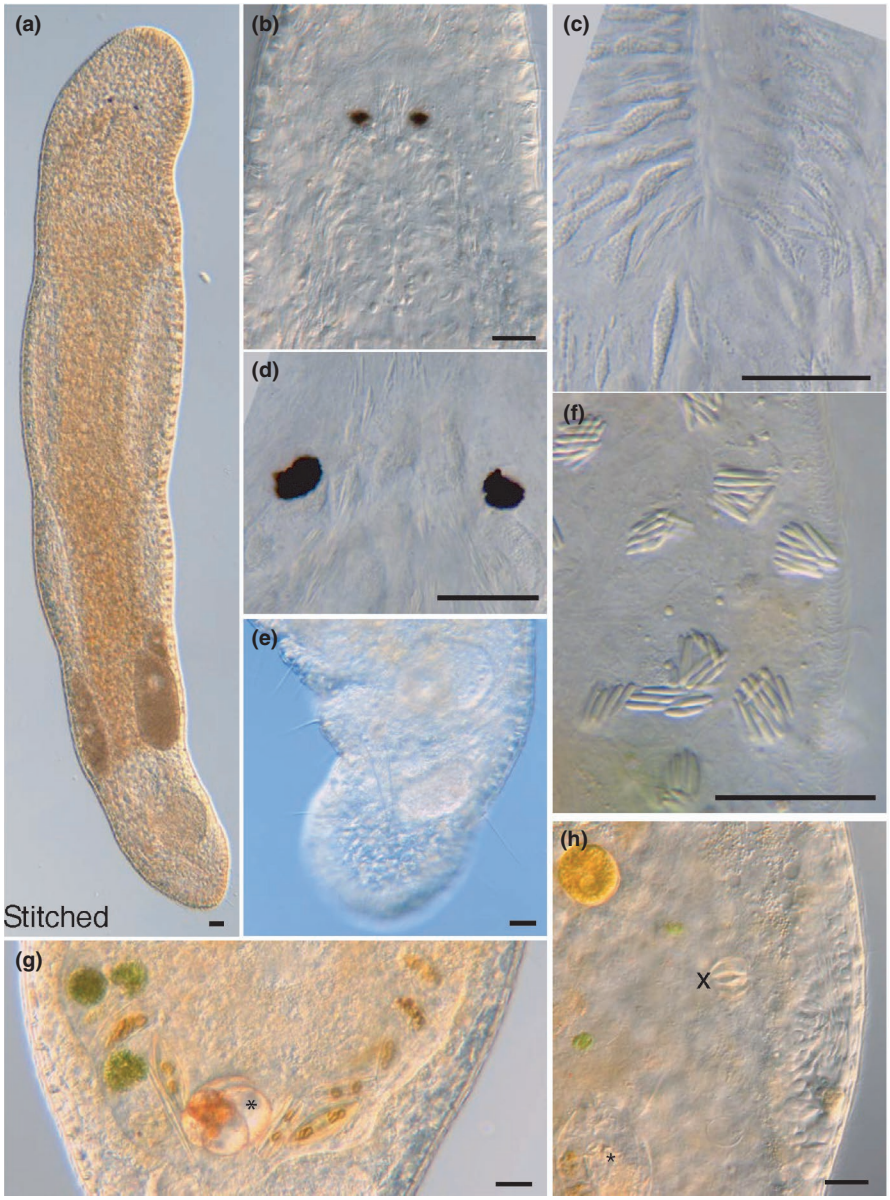

FIGURE 5 Micrographs of somatic structures of *Macrostomum cliftonensis* collected from the field (the bracket denotes the code of the deposited specimen, with MTP LS 2986 being the HOLOTYPE; note that all these specimens were imaged from the ventral side). (a) Overview of an adult, lightly squeezed, worm (MTP LS 2920, stitched from 3 images); (b) head region with neuropile, eyes, and pharynx (MTP LS 2930); (c) mouth opening with two distinct pharyngeal gland secretions (MTP LS 2911); (d) eyes with rhammite gland secretions penetrating the neuropile (MTP LS 2911); (e) tail region with numerous long sensory hairs (MTP LS 2906); (f) rhabdite bundles and ciliated epidermis (MTP LS 2930); (g) gut content with green algae, diatoms, and a foraminifer (*) (MTP LS 2910); (h) details of gut contents with a partially digested rotifer (*) and a rotifer jaw (x) (MTP LS 2930; for more detail see also 2017-01-18_19-37-08.074.avi). Scale bars 25 μm

center of mass (see also Figure 11a drawn from a more detailed recording). At the end of the copulation, one worm swims away, while the other remains at the same spot. At 189 s, the worms again come into contact and engage in circling, resulting in an unsuccessful copulation attempt at 212 s. This is followed by the bottom worm swimming away (at 248 s) and sucking (at 267 s) for a duration of 11 s (see also Figure 11b drawn from a more detailed recording).

Karyology and genome size. As already shown by Zadesenets et al. (2016), the most common karyotype of *M. janickei* (called *Macrostomum* sp. 8 therein) is 2n = 10 (18/22 specimens or 81.2%), with six small and four large metacentric chromosomes (Figure 11a), but there were also two specimens each that had either three (2n = 9) or five (2n = 11) large chromosomes (Figure 11b). The flow cytometric genome size estimates of *M. janickei* showed a complex pattern that approximately matched our karyotype results (Figure S1), with the most prominent peak having a relative fluorescence that was on average 4.55× larger than that of *D. melanogaster*, which would therefore correspond to a haploid genome size in *M. janickei* of 779 Mbp. However, note that these large chromosomes appear to represent near identical copies (Zadesenets, Schärer, et al., 2017b; Zadesenets et al., 2016), so that the actual amount of unique genome sequence might be lower. More detailed analyses of the genome organization of *M. janickei* are underway (K. S. Zadesenets, I. E. Jetybayev, L. Schärer, & N. B. Rubtsov, unpublished data).

Discussion

Given its characteristic stylet, *M. janickei* is clearly distinct from all other species in the genus *Macrostomum* published to date. The only species whose stylets bear any resemblance are *M. hamatum* Luther, 1947, described from the Baltic Sea at Tvärminne, Finland (Luther, 1947), one of the drawings of *M. balticum meridionalis* Papi, 1953, described from the San Rossore park near Pisa, Italy (Papi, 1953),

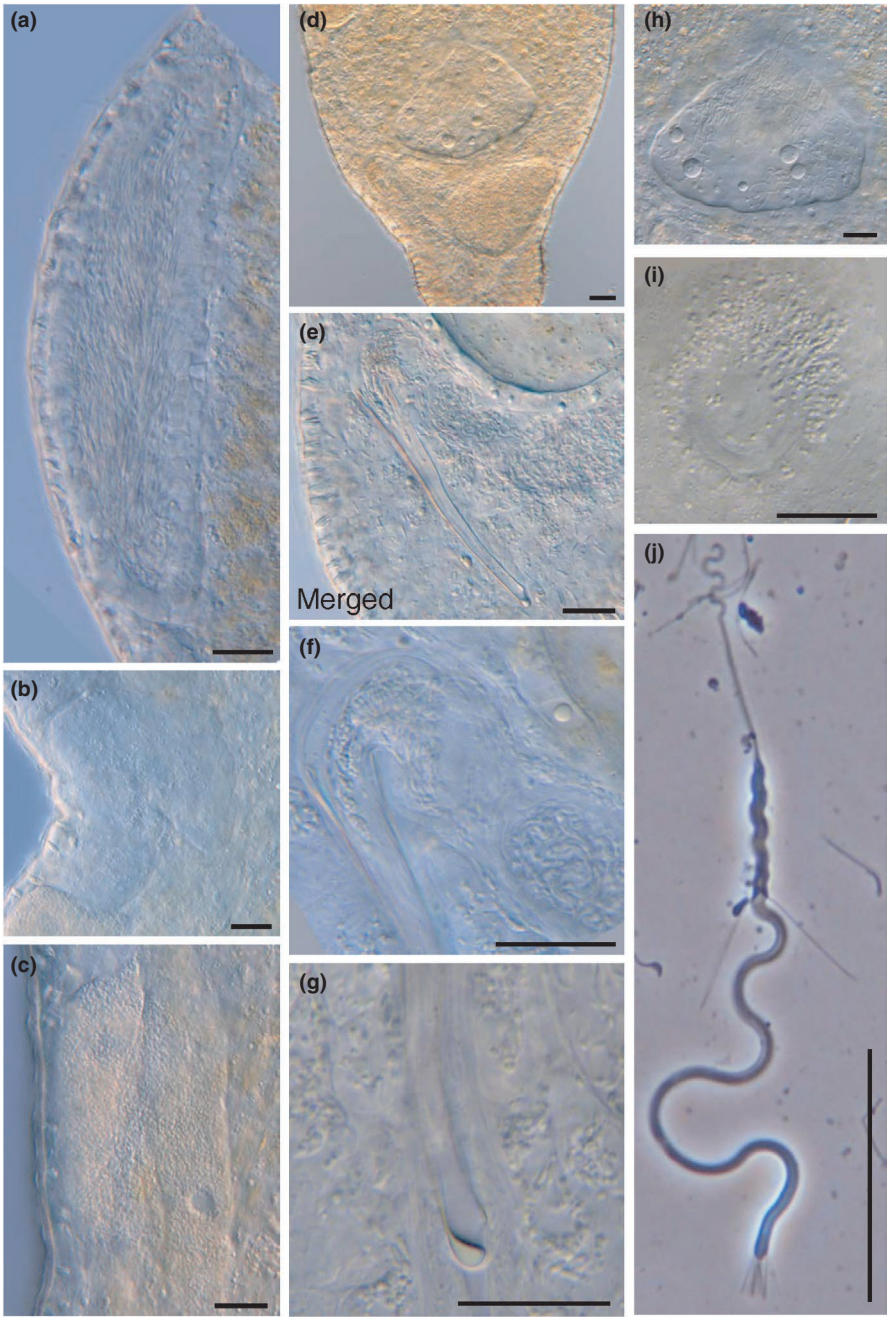

FIGURE 6 Micrographs of reproductive structures of *Macrostomum cliftonensis* collected from the field (the bracket denotes the code of the deposited specimen, with MTP LS 2986 being the HOLOTYPE; note that all specimens, except MTP LS 2908, were imaged from the ventral side). (a) Ripe testis with elongating spermatids aligned in the central region (MTP LS 2907); (b) ripe ovary with oocytes that are beginning to form yolk and shell granules (MTP LS 2896); (c) forming egg with the clearly visible nucleus, and many yolk and shell granules (MTP LS 2896); (d) body region containing the female antrum, the false and true seminal vesicle, vesicula granulorum, and stylet (MTP LS 2896); (e) false and true seminal vesicle, vesicula granulorum, and stylet (MTP LS 2907, merged from a movie); (f) muscular true seminal vesicle, ductus intervesicularis, vesicula granulorum, and base of the stylet (MTP LS 2907; see also the 2017-01-17_18-40-30.180.avi for additional detail); (g) tip of the stylet showing asymmetrical distal thickening (MTP LS 2911; for more detail see also 2017-01-18_10-53-55.330.avi); (h) female antrum with received sperm and coagulated seminal fluid; note the ciliary tuft in the center (MTP LS 2896). (i) Vagina surrounded by shell glands; note that the anterior shell glands appear first when focusing into the antrum (MTP LS 2896). (j) Sperm with typical feeler, body, bristles, shaft, and brush (MTP LS 2908, frame extracted from a movie). Scale bars 25 µm

specifically Figure 11 of Papi, 1953, and to a lesser degree *M. reynoldsoni* Young, 1976, described from the river Mwena near Mombasa, Kenya. We discuss these in turn in the following.

While the stylet of *M. hamatum* also has a hook-like appearance on the distal end, the stylet is more slender and has a fairly steady crescent-like turn of the stylet shaft. While Luther does not give any stylet length measurements, Ax (2008) reports on specimens collected in Sylt, Germany, that reach lengths of up to 150 µm, thus greatly exceeding the values of *M. janickei*. Moreover, we collected *M. hamatum* several times close to the type locality in Finland and find similar stylet lengths in our specimens. Finally, ongoing molecular phylogenetic analyses clearly show that *M. hamatum* is distinct from *M. janickei* (J. N. Brand, & L. Schärer, unpublished data). It is tempting to speculate that the stylet morphology of *M. janickei* might be involved in accessing difficult to reach parts of the female antrum, in order to remove rival sperm or lodge own sperm into places where they can efficiently anchor themselves with their feelers.

In the description of *M. balticum meridionalis*, Papi (1953) presents several drawings of the stylet, only one of which bears any resemblance to *M. janickei*, namely his Figure 11 (a reconstruction for serial sections). While all the other drawings of this species (Figures 6–9) clearly show a subterminal opening and a large unilateral distal thickening that exits at an angle <90° (a character state shared with *M. balticum* Luther, 1947, the species Papi considers his to be a subspecies of), the distal tip in Figure 11 is not drawn in much detail, and could possibly show a >90° turn, but leaving the placement of

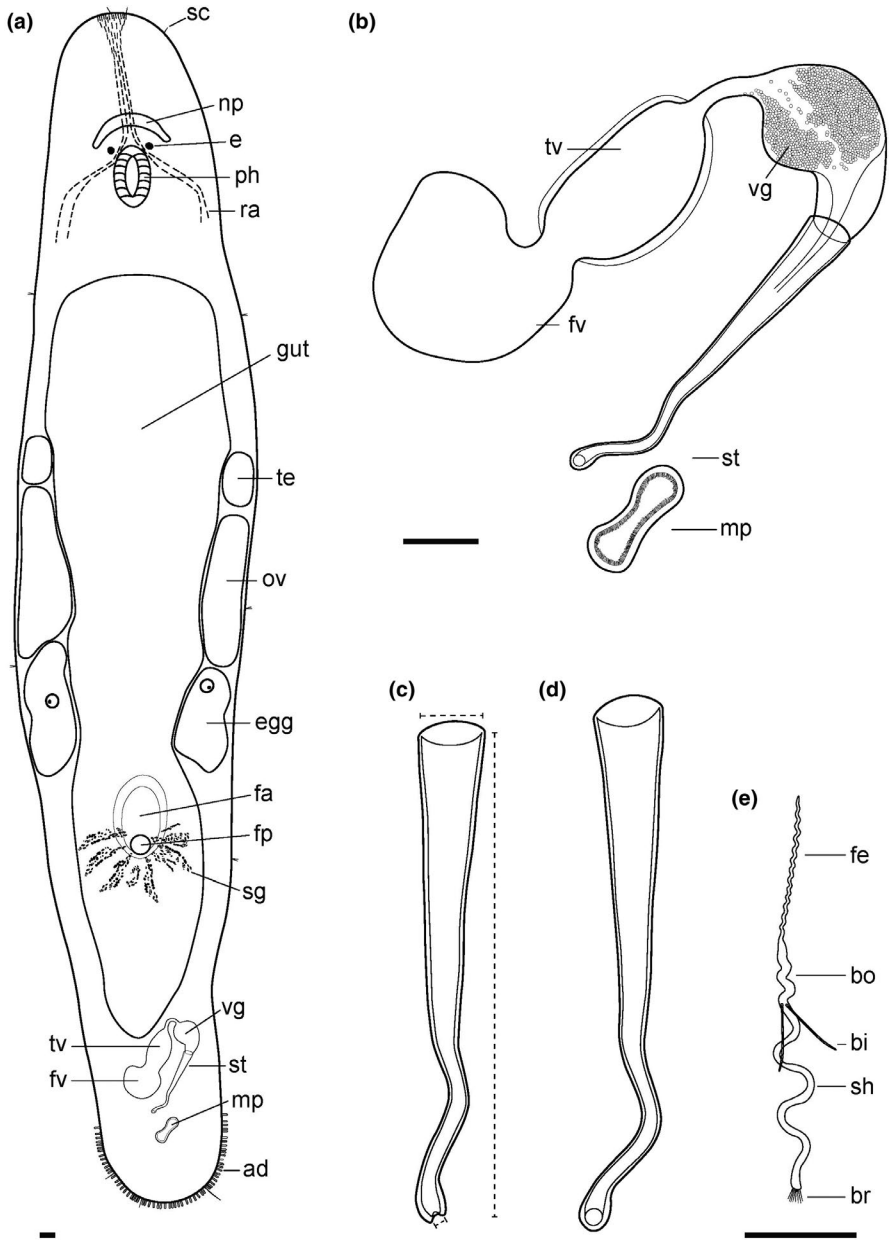

FIGURE 7 Line drawings of *Macrostomum mirumnovem* n. sp.: (a) Habitus (viewed from dorsal and lightly squeezed). (b) Male genital system with false seminal vesicle, muscular true seminal vesicle, vesicula granulorum, and stylet. (c) Detailed drawing of a common view of the stylet. (d) Detailed drawing of an alternate view of the stylet. (e) Mature sperm cell with feeler, body, bristles, shaft, and brush (see Figure 1 for abbreviations)

the opening unclear. Given the difficulties in reconstructing complex shapes of small (5–10 μm) structures from relatively thick paraffin sections (those of Papi are 3–4 μm, L. Schärer, pers. obs.), and given the fairly consistent stylet tip morphology in the other drawings, Figure 11 should clearly not be considered diagnostic for the stylet tip. Moreover, *M. balticum* has previously been phylogenetically placed close to *M. spirale* Ax, 1956, forming a clade that is quite diverged from the clade containing *M. janickei* (and *M. lignano* and *M. hystrix*), and we have ourselves recently collected *M. balticum meridionalis* close to the type locality, based on which we will show that, while being close to *M. balticum*, it is clearly a separate species (J. N. Brand, & L. Schärer, unpublished data).

While the stylet of *M. reynoldsoni* also turns >90° close to the distal tip, it does so in a much more gradual way than what we see in *M. janickei* and *M. hamatum*, leading to a nearly complete semicircle, rather than a sharp point. Moreover, the stylet of *M. reynoldsoni* lacks the "slight turn of about 40° at about 80% of its length" that we consider diagnostic for *M. janickei*.

Given that *M. janickei* is the closest relative of *M. lignano* found to date, we compared their mating behavior in pure versus mixed pairs and found that while both the copulation and suck durations were significantly longer in *M. janickei* than in *M. lignano*, these species are capable of cross-species mating, leading to low levels of successful hybridization (P. Singh, D. Ballmer, M. Laubscher, & L. Schärer, unpublished data), which further supports that they are phylogenetically closely related. Intriguingly, the resulting hybrid offspring showed an intermediate stylet morphology (P. Singh, D. Ballmer, M. Laubscher, & L. Schärer, unpublished data). Given what we currently know about the distribution of these species, it is unclear if there might be a naturally occurring hybrid zone.

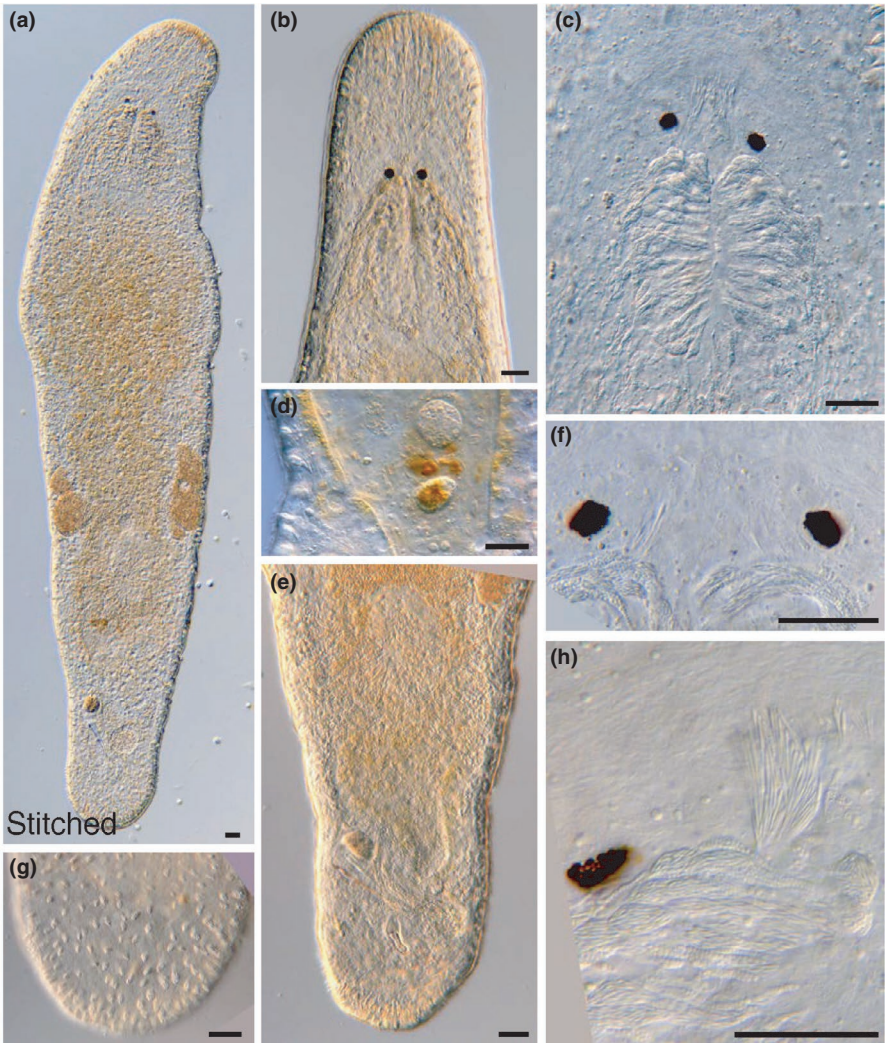

FIGURE 8 Micrographs of somatic structures of *Macrostomum mirumnovem* collected from the field (the bracket denotes the code of the deposited specimen, with MTP LS 3014 being the HOLOTYPE; note that all specimens, except MTP LS 3012, were imaged from the ventral side). (a) Overview of an adult, lightly squeezed, worm (MTP LS 3015, stitched from three images); (b) head region with rhammite glands, neuropile, eyes, and pharynx (MTP LS 3012); (c) pharynx region with neuropile, eyes, pharynx gland necks, and mouth opening (MTP LS 3015, frame extracted from a movie); (d) gut content with diatoms, and an unknown round cellular structure (MTP LS 2995, frame extracted from a movie); (e) tail region with adhesive glands (MTP LS 2993); (f) eyes with a few rhammite gland secretions penetrating the neuropile (MTP LS 3014); (g) rhabdite bundles on the tail plate (MTP LS 2996); (h) details of the pharynx gland necks showing two distinct pharyngeal gland secretions, as well as one pigment cup and some rhammite gland secretions (MTP LS 2994). Scale bars 25 μm

Macrostomum cliftonensis Schärer & Brand, n. sp.

urn:lsid:zoobank.org:act:18D35DE3-DE39-4E2A-9931-01499ABECA59 (Figures 4–6, Figure 10c, d, Figure 11c, d; Table 1, Table 2)

Material examined. Live observations on 14 field-collected specimens. Holotype: one extensively documented worm (MTP LS 2896, 94 images and videos) from the type locality (i.e., sample G7 collected on 17 January 2017 from sandy shore with reduced salinity water of 35‰ salinity seeping into a puddle on the shores of the increasingly hypersaline Lake Clifton with 97‰ salinity at time of sampling, Western Australia; S 32.76125, E 115.66019), including a whole mount (WAM V9393) and both partial *28S rRNA* and *COI* gene sequences. Paratypes: 13 extensively documented specimens (for a total of 724 images and videos), which complement the characterization of the holotype (see also Table 2), and many of which were also sequenced and/or include whole mounts.

Etymology. Species name refers to the type locality. To facilitate backward compatibility with previous records and reports, we note that this species has previously been referred to as *Macrostomum* sp. 84 (or Mac084 for short).

Diagnosis. *Macrostomum* with slightly dorsoventrally flattened and tongue-shaped body, and rounded rostrum (Figure 4a; Figure 4a). Body lengths of field caught worms range from 709 to 1,762 μm (see also Table 2). Short and long sensory cilia, with former mainly on anterior body and latter particularly pronounced on tail plate. Two small pigment cup eyes that sometimes appear kidney-shaped. Mouth relatively long, and gut extending caudally beyond female antrum, but posterior part relatively inconspicuous. Plentiful rhabdite bundles all over body, both on the dorsal and ventral side. Testes clearly larger than ovaries. The stylet is a long (~120 μm), slender and gradually narrowing funnel that, when looked at laterally, includes a slight turn (of ~15°) in about the center (although the stylet is also slightly curved at a right angle to this axis). Stylet ends in an oblique and almost lateral distal opening, with outside showing drop-shaped thickening and inside barely thickened (Figures 4c, 6g). Vesicula granulorum stands at a >90° angle to stylet axis. Vagina central, and received sperm can often be observed in female antrum, being anchored with feelers inside cellular valve. Shell glands granules surrounding vagina first appear in the anterior region when one focusses into antrum. Sperm relatively long (103 μm) showing general morphology of reciprocally mating species (Schärer et al., 2011).

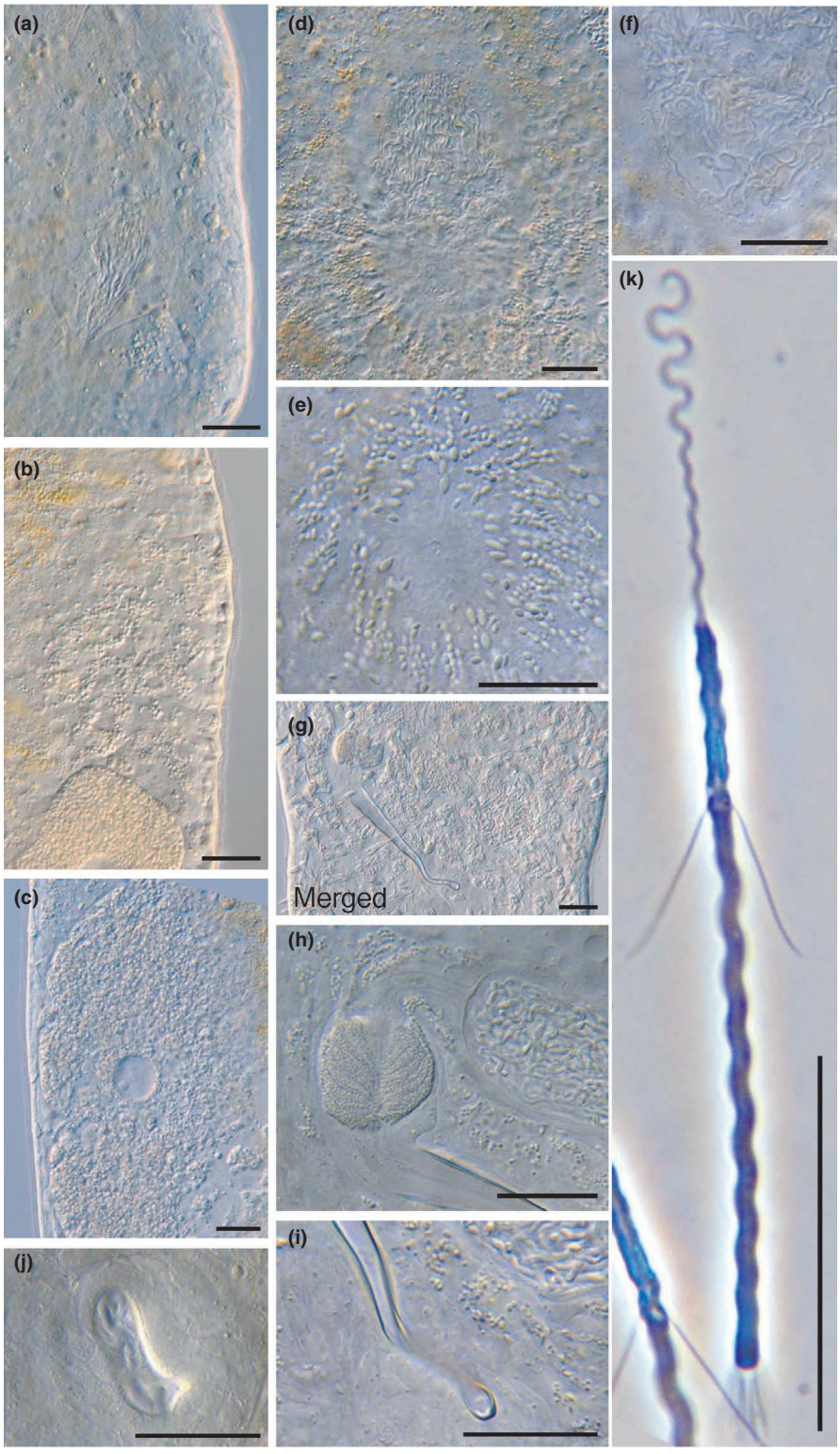

FIGURE 9 Micrographs of reproductive structures of *Macrostomum mirumnovem* collected from the field (the bracket denotes the code of the deposited specimen, with MTP LS 3014 being the HOLOTYPE; note that all these specimens were imaged from the ventral side). (a) ripe testis with some elongating spermatids aligned in the central region and the start of the vas deferens (MTP LS 3016); (b) ripe ovary with oocytes that are beginning to form yolk and shell granules, and a forming eggs (MTP LS 2994); (c) forming egg with the clearly visible nucleus and nucleolus, and many yolk and shell granules (MTP LS 3014); (d) body region containing the female antrum, the vagina and the shell glands (MTP LS 3015, frame extracted from a movie); (e) vagina surrounded by shell glands (MTP LS 3015, frame extracted from a movie). (f) Posterior region of the female antrum with received sperm, some coagulated seminal fluid; note the ciliary tuft left of the center (MTP LS 3015, frame extracted from a movie). (g) False and true seminal vesicle, vesicula granulorum, and stylet (MTP LS 3014, merged from a movie); (h) muscular true seminal vesicle, ductus intervesicularis, vesicula granulorum, and base of the stylet (MTP LS 3015); (i) tip of the stylet showing considerable s-shaped curvature and weak distal thickenings (MTP LS 3015, frame extracted from a movie); (j) the unusually large opening of the male antrum, lined by many cilia (MTP LS 2993, frame extracted from a movie). (k) Sperm with typical feeler, body, bristles, shaft, and brush (MTP LS 2993, frame extracted from a movie). Scale bars 25 μm

Description (see also Table 2)

General morphology. The body is slightly dorsoventrally flattened and tongue-shaped (width/length ratio: 1:3.8), and widest at the level of testes or ovaries (Figures 4a, 5a). The rostrum is rounded and the tail plate barely set apart from the rest of the body. The pigment cup eyes are small and often slightly kidney-shaped (Figure 5d). The body is covered homogeneously with cilia, and short sensory cilia are present on the rostrum, while there are sparse long sensory cilia all along the body, particularly on the tail plate (Figure 5e). The pharynx is associated with a relatively long mouth opening (Figure 5b, c), and the gut (often containing food items, Figure 5g, h) extends posteriorly beyond the female antrum, ending at the seminal vesicles (at 85% BL). There are many rhabdite bundles all over the body, both on

the dorsal and ventral side (with the exception of the regions around the mouth and the gonopores), forming bundles of 6–13 granules (Figure 5f). The rhammite glands originate dorsally anterior of the testes, and their granules are secreted via the neuropile (Figure 5b) into the anterior rostrum, where very prominent rhammite bundles can be observed. The adhesive glands are arranged horseshoe-like in multiple rows along the edge of the tail plate.

Male system. The prominent testes extend from 30% to 48% BL, with developing sperm aligned in the center (Figure 6a). The vas deferens can be seen in some specimens (e.g., MTP LS 2909) and appears to leave the testis at the posterior end. There is a prominent and often oval-shaped false seminal vesicle that lies on the left of the tail plate and which often extends quite far posterior (Figure 6d). It connects anterolaterally to a muscular true seminal vesicle that lies in a more central position. The true seminal vesicle is connected anterolaterally via a short ductus intervesicularis to the prominent and muscular vesicula granulorum (Figures 4b; 6e, f), whose main axis is positioned on the proximal stylet opening at a >90° angle to the main axis of the stylet. The tail plate contains many prostate gland cells that send out their necks into the vesicula granulorum, from which prostate glands necks only reach into the first ~15% of the stylet length (Figure 6f). The stylet is a very slender and gradually narrowing funnel that, when looked at laterally, includes a very slight turn of about 15° at about 60% of its length, before then ending in an oblique and almost lateral distal opening (Figures 5c, 6f); note, however, that the stylet is also slightly curved at a right angle to this axis, which can be seen in the second drawing (Figure 4d). The outside of the distal end shows a drop-shaped thickening, while the inside is barely thickened (Figures 4c, 6g); note that stylet and tip can appear quite differently when somewhat rotated (see Figure 4d). The male canal ends in a distinct male antrum, and the male gonopore (at 95% BL) is ciliated. The sperm (Figures 4e, 6j) have the usual morphology for a species in the reciprocally mating clade (Schärer et al., 2011).

Female system. The ovaries lie directly behind the testes (from 49% to 62% BL) and show the usual morphology (Figures 4a, 6b), and the developing eggs also show the usual structure, with ample yolk and shell granules (Figure 6c). The female antrum lies centrally and appears somewhat variable in shape, often having a distinct lumen and a prominent anterior thickening of the epithelium (Figure 6d + h). The vagina opens directly into the antrum lumen (at 80% BL). Received sperm can often be observed being anchored with their feelers inside of the cellular valve; note that one can often observe coagulated prostate secretions (Figure 6d + h). Where the vagina enters the female antrum, there is a distinct ciliary tuft with long cilia that reach into the antrum lumen (Figure 6h). Shell glands surround the vagina, with the granules first appearing in the anterior region when one focusses into the antrum (Figure 6j). The shell gland secretions are remarkably dense, but do not extend far from the female opening, rarely reaching the sides of the animal.

Mating behaviour. In Video S2, the worms get into contact at 6 s, leading to the initiation of precopulatory behavior at 47 s, in which the worms circle and crawl on each other for 23 s. From 70 s, the worms are firmly interlinked in a disk-like posture and start copulating. The copulation lasts for ~34 s and ends at 105 s, during which the worms rotate about their center of mass, followed by both worms sucking (at 105 s) for a duration of 10 and 14 s, respectively.

Karyology and genome size. All 100 analyzed specimens of *M. cliftonensis* showed a 2n = 6 karyotype with six similar-sized metacentric chromosomes (Figure 11c-d) and that simple karyotype was also supported by our flow cytometric genome size estimates (Figure S1). These showed a single peak having a relative fluorescence that was on average 1.35× larger than that of *D. melanogaster*, which would therefore correspond to a haploid genome size in *M. cliftonensis* of 231 Mbp. More detailed analyses of the genome organization of *M. cliftonensis* are underway (K. S. Zadesenets, I. E. Jetybayev, L. Schärer, & N. B. Rubtsov, unpublished data).

Discussion

As shown in Figure 4c, d, the stylet of *M. cliftonensis* can appear somewhat variable in different specimens, which is, at least in part, due to the angle at which these stylets are viewed. Moreover, in one deposited specimen (MTP LS 2920) the stylet appears malformed and shorter than usual, possibly because the initial elongation during stylet formation was hampered (stylets start forming from the distal tip; Egger et al., 2009), leading to a mass of accumulated stylet material at the distal tip.

While the stylet of *M. cliftonensis* is unique, there are five *Macrostomum* species with stylets that are similar, all of which match by inhabiting coastal brackish habitats. First, *M. curvituba* Luther, 1947—described from the Hanko peninsula, Finland—differs by being blind and having a stylet that is smaller (75–103 µm), more evenly curved and ending in bilateral distal thickenings (Ax, 1994; Luther, 1947). Second, *M. magnacurvituba* Ax, 1994—described from coastal waters of Greenland and Iceland—is also blind and has a stylet that is somewhat similar but much larger (140–175 µm) than either *M. curvituba* (hence the name; Ax, 1994) or *M. cliftonensis*. Third, *M. mediterraneum* Ax, 1956—described from Etang de Sigean, Southern France—has a stylet that matches *M. cliftonensis* by being somewhat (although fairly evenly) curved and having a unilateral distal thickening. However, Ax actually draws this distal thickening of this species somewhat differently in different papers, being smaller and more similar to *M. cliftonensis* in the initial description (Ax, 1956), and larger and more rounded (and thus less similar) in a later account from the Marmara Sea, Turkey (Ax, 1959). Moreover, in both cases these stylets are either shorter (88–90 µm) or in the lower range (103 µm), respectively, than that of *M. cliftonensis*. Fourth, *M. longituba* Papi, 1953—described from a brackish water canal in the San Rossore Reserve, Pisa—has a stylet that is not only more evenly curved and longer, but also ends in a much narrower tip that lacks a very distinct distal thickening and includes a slight turn at the very end (Papi, 1953).

Finally, *M. greenwoodi* Faubel & Cameron, 2001—described from the Coomera salt marshes, Queensland—is superficially the most similar species, and since it was described from coastal habitats in

Queensland, Australia (Faubel & Cameron, 2001), we discuss it in some more depth. In overall appearance, the two species are similar, with the reported body length of 980 µm being within the range of *M. cliftonensis*, and with the distribution of sensory cilia and rhabdites approximately matching as well. The stylet of *M. greenwoodi* is more evenly and more strongly curved, and reported to be shorter than that of *M. cliftonensis*, with values in the text given as 98.3 µm, although Figure 3a, b of Faubel (2001) suggest conflicting values of 105 µm and 53 µm, respectively. For the following comparison, we assume that this discrepancy stems from the scale bar of Figure 3b being wrong, suggesting a stylet length of ~100 µm, which is also supported by a re-examination of the serially sectioned holotype of *M. greenwoodi* (Queensland Museum, QMG217363), which Ladurner et al. (2005) carried out as part of their species description of *M. lignano*. This stylet size is in the lower range of what we have found in *M. cliftonensis* (though note that our shortest stylet may have been malformed). Moreover, in *M. greenwoodi* the size of the proximal opening (13 µm) as well as the distal opening (4 µm) is, respectively, just outside and just inside the range of what we observe in *M. cliftonensis*, suggesting that the stylet of *M. greenwoodi* is overall smaller and narrower, as well as more evenly and strongly curved. And while Faubel does not mention distal thickenings of the stylet tip, the re-examination of the holotype had actually suggested that this species does carry thickenings (Ladurner et al., 2005). Other aspects that do not match well are the positions of the female and male gonopores, which are both more anterior in *M. greenwoodi* (70% and 91%) compared to *M. cliftonensis* (82% and 95%). And finally, Faubel (2001) does not draw cilia that surround the region where the vagina enters the female antrum (and this absence was confirmed by the re-examination of the holotype; Ladurner et al., 2005), while we clearly see such cilia in *M. cliftonensis*. We therefore conclude that *M. cliftonensis* is distinct from *M. greenwoodi*, and all the other species discussed above.

Macrostomum mirumnovem Schärer & Brand, n. sp.

urn:lsid:zoobank.org:act:740C2A0B-8288-4CB6-9E09-0959A4338120
(Figures 7–9, Figure 10e, f, Figure 11e, f; Table 1, Table 2)

Material examined. Live observations on 11 field-collected specimens and one specimen from laboratory culture. Holotype: one extensively documented worm (MTP LS 3014, 68 images and videos) from the type locality (i.e., sample A13 collected on 29 January 2017 from the upper intertidal on a sheltered beach, at 35‰ salinity, in front of the Victorian Marine Science Consortium, Queenscliff, Port Phillip Bay, Victoria; S 38.27007, E 144.63894), including a whole mount (NMW F258462). Paratypes: 11 extensively documented specimens, some from the type locality and others from other locations in the general area (for a total of 579 images and videos), which complement the characterization of the holotype (see also Table 2), and many of which were sequenced and/or include whole mounts.

Etymology. Species name refers to unusual karyotype that generally consists of nine chromosomes (Lat. *mirum* = strange and *novem* = nine). To facilitate backward compatibility with previous records and reports, we note that this species has previously been referred to as *Macrostomum* sp. 94 (or Mac094 for short).

Diagnosis. *Macrostomum* species with slightly dorsoventrally flattened and lancet-shaped body, conical rostrum with frequently rounded tip, and tail plate being slightly set aside (Figures 7a, 8a). Body lengths of field caught worms range from 670 to 1,667 µm (see also Table 2). Short and slightly longer sensory cilia, with former mainly on anterior body and latter only on tail plate. Two small pigment cup eyes that sometimes appear crescent-shaped. Gut extending caudally far beyond female antrum. Testes clearly smaller than ovaries. The distinctive stylet (~80 µm) is a slender and gradually narrowing funnel that then stays relatively constant in diameter in distal half, widening again near tip (Figures 7c, 9g), multiple turns in s-shaped mid region, occurring in more than one plane (compare views in Figure 7c, d). Depending on viewing angle, the distal stylet opening ends terminally or somewhat subterminally, both sides carrying slight distal thickenings (Figure 9i). Prostate gland cells send out necks into vesicula granulorum, but granules do not reach into stylet, while a set of strong muscles do. Vagina central and received sperm can often be observed in the female antrum, anchored with feelers inside cellular valve. Dense shell glands surround vagina, with majority radiating laterally, none directly anterior and only few posterior. Sperm (86 µm) showing the general morphology of reciprocally mating species (Schärer et al., 2011), having a relatively long feeler (32 µm).

Description (see also Table 2)

General morphology. The body is slightly dorsoventrally flattened and lancet-shaped, and widest at the level of the testes (Figures 7a, 8a). The rostrum is conical and the tip often rounded (Figure 8b), and the tail plate is slightly set aside (Figure 8e). The pigment cup eyes are small and often crescent-shaped (Figure 8c + f + h). The body is covered homogeneously with cilia, and sparse sensory cilia are largely restricted to the rostrum, with a few slightly longer ones on the tail plate. The mouth and pharynx are unremarkable (Figure 8b, c), and the gut extends posteriorly far beyond the female antrum (sometimes containing food items, Figure 8d + e), ending directly at the seminal vesicles (at 83% BL). Rhabdite bundles are relatively sparse, and most abundant on the dorsal side of the head and tail, forming bundles of 4 to 12 granules (Figure 8g). The rhammite glands originate dorsally anterior of the testes, and their granules are secreted via the neuropile into the anterior rostrum, where prominent rhammite bundles can be observed (Figure 8b, c). The adhesive glands are arranged horseshoe-like in multiple rows along the edge of the tail plate.

Male system. The small and often difficult to see testes extend from 31% to 38% BL and they usually show relatively few developing sperm that are often curled up in the center (Figure 9a). While the vas deferens is not easily seen, one can sometimes see a few ripe sperm descending toward the seminal vesicles. There is a small false seminal vesicle that lies on the left of the tail plate and which connects anterolaterally to a more central muscular true seminal vesicle (Figures 7b, 9g). The true seminal vesicle is connected via

a ductus intervesicularis that turns sharply into the prominent and muscular vesicula granulorum, which itself sits on the proximal stylet opening at a considerable angle (Figure 9h). The tail contains many prostate gland cells that send out their necks into the vesicula granulorum, but the granules do not reach into the stylet, while a set of strong muscles do (Figure 9h). Besides these distal muscles, the vesicula granulorum does not show signs of strong musculature. The stylet is a slender and gradually narrowing funnel for the first 60% of its length that then stays relatively constant in diameter for the next 35% in the mid region, and finally widening again near the tip (Figures 7c, 9g); there are multiple turns in this s-shaped mid region, the first by about 20° and the second, turning back by about 60°, but the turns occur in more than one plane, and can therefore not be completely captured in 2D (compare the views in Figure 7). Depending on the viewing angle, the distal stylet opening ends terminally or somewhat subterminally (compare Figure 7c, d), and both sides carry slight distal thickenings (Figure 9i). The male canal ends in a remarkably spacious male antrum, and the male gonopore is unusually large, often forming an oblong slit (Figure 9j); both the male antrum and the male pore (located at 92% BL) are strongly ciliated. The sperm (Figures 7e, 9k) have the usual morphology for a species in the reciprocally mating clade (Schärer et al., 2011).

Female system. The prominent ovaries lie directly behind the testes (from 39% to 54% BL) and show the usual morphology (Figure 9b), and the developing eggs show the usual structure, with ample yolk and shell granules (Figure 9c). The female antrum lies centrally, is relatively simple, oblong and has a thick antrum epithelium (Figure 9d). The vagina also lies centrally, entering in the posterior section of the antrum (at 68% BL). Received sperm can often be observed being anchored with their feelers inside the cellular valve. Where the vagina enters the female antrum, there is a small ciliary tuft with cilia that reach into the antrum lumen (Figure 9f). Dense shell glands surround the vagina and they extend asymmetrically, with the majority radiating laterally, none directly anterior and only few posterior (Figure 9e).

Mating behaviour. In Video S3, the worms come into contact at 8 s and begin to circle each other, potentially trying to get into the copulatory posture. At 15 s, they start reciprocally copulating for a duration of 803 s, though by 791 s the copulation seems unilateral, with the worm on the right presumably having removed its stylet from the partner's female antrum. Their copulatory posture appears angular, with the shape resembling an **S** (see e.g. at 529 s). At the beginning of the copulation, the worms vigorously move and elongate their anterior body (at 8–78 s), but this eventually slows down. At 832 s, the worm on the left bends down and starts sucking for a duration of 14 s.

Karyology and genome size. The most common karyotype of *M. mirumnovem* is 2n = 9 (34/52 specimens or 65.4%) with six small and three large metacentrics (Figure 11e). However, there are a large number of specimens, which differ both in the number of small and large chromosomes (K. S. Zadesenets, I. E. Jetybayev, L. Schärer, & N. B. Rubtsov, unpublished data). Surprisingly, the flow cytometric genome size estimates of *M. mirumnovem* showed an apparently simpler pattern than what we could have expected based on our karyotype results (Figure S1), with only a single peak having a relative fluorescence that was on average 2.52× larger than that of *D. melanogaster*, and which would therefore correspond to a haploid genome size in *M. mirumnovem* of 431 Mbp. However, given some caveats regarding the measurements for this species, these values need to be treated with some caution (see Figure S1). More detailed analyses of the genome organization of *M. mirumnovem* are underway (K. S. Zadesenets, I. E. Jetybayev, L. Schärer, & N. B. Rubtsov, unpublished data).

Discussion

While the complex stylet shape of *M. mirumnovem* is unique, there are four described species that have comparably complex stylets, two each inhabiting freshwater and coastal brackish habitats, respectively. The former includes *M. johni* Young, 1972—described from a freshwater lake in Wales (Young, 1972), but also reported from a freshwater coastal lagoon in Brazil (Gamo & Leal-Zanchet, 2004)—has a stylet that is similar in size (78–95 µm) to that of *M. mirumnovem*. Its stylet also shows multiple complex turns, but ends in "a slightly swollen cowl or hood" (Young, 1972), and thus is clearly distinct from our species. Moreover, in *M. johni* the testes are almost twice as long as the ovaries, while the reverse is true for *M. mirumnovem*, and the female antrum is considerably further back in *M. johni* and the gut ends approximately at the level of the antrum. The other freshwater species, *M. retortum* Papi, 1951—described from temporary freshwater ponds in the San Rossore Reserve, Pisa—has a stylet that is not only more complex, but also considerably longer (up to 138 µm) than that of *M. mirumnovem* (Papi, 1951).

Among the coastal species, *M. bellebaruchae* Ax, 2008—described from Winyah Bay, South Carolina in freshwater, but considered to have some brackish influence—has a stylet that also has many turns, but is considerably shorter (56 µm) than that of *M. mirumnovem* and does not carry any distal thickenings on the stylet tip (Ax, 2008). The other brackish species is *M. coomerensis* Faubel & Cameron, 2001—collected from the Coomera salt marshes, Queensland—whose stylet resembles an exaggerated version of that of *M. mirumnovem*, both with respect to the more acute sharpness of the many turns, as well as with respect to its much larger size (125 µm), and the more extreme turn at the end, leading to a clearly subterminal opening (Faubel & Cameron, 2001).

Karyotype and genome size of *Macrostomum lignano* and *Macrostomum hystrix*

As shown previously (and briefly summarized above), *M. lignano* has a complex karyotype, with different inbred lines and outbred cultures showing different levels of karyotype variability (Zadesenets et al., 2016). These observations are well supported by the flow cytometric genome size estimates we obtained here (Figure S1), with the DV1 inbred line and the LS3 outbred culture showing peaks that correspond to the known 2n = 8, 2n = 9, and 2n = 10 karyotypes, and the LS1 outbred culture showing a single peak corresponding

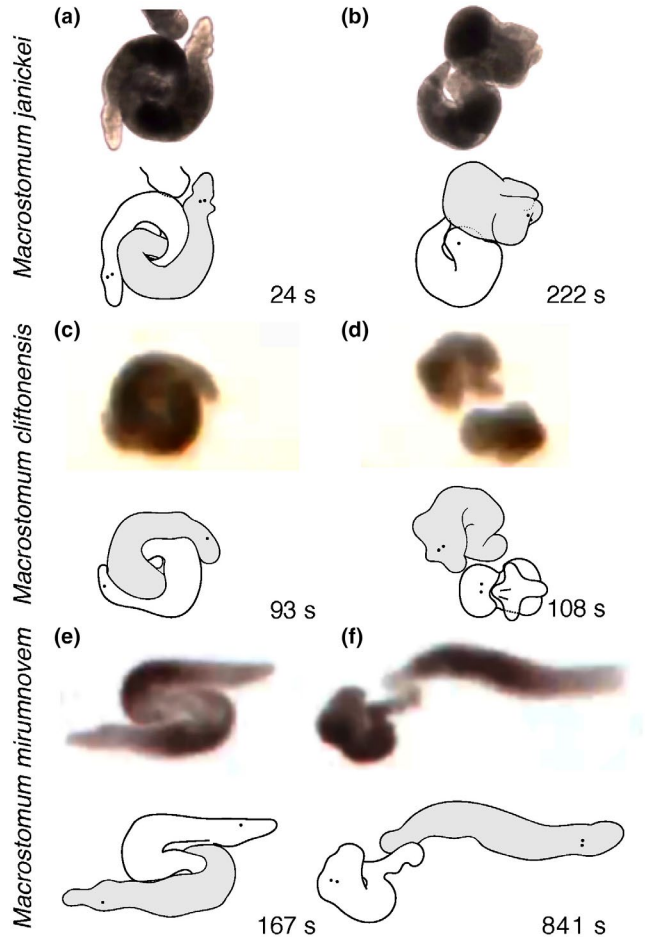

FIGURE 10 Mating behavior of three new *Macrostomum* species, with single frames extracted from the deposited movies and line drawings made from these frames: (a) copulatory posture of *M. janickei* (frame taken from an additional movie that had contained three worms); (b) sucking behavior of *M. janickei* (frame taken from an additional movie), with the upper worm showing the suck posture oriented obliquely; (c) copulatory posture of *M cliftonensis*; (d) sucking behavior of *Macrostomum cliftonensis*, with the upper and lower worms showing the suck posture oriented sideways and toward the camera, respectively; (e) copulatory posture of *M. mirumnovem*; and (f) sucking behavior of *M. mirumnovem*, with the left worm showing the suck posture oriented sideways. Note that the timing information refers to the deposited movies and that the magnifications are not to scale across the species

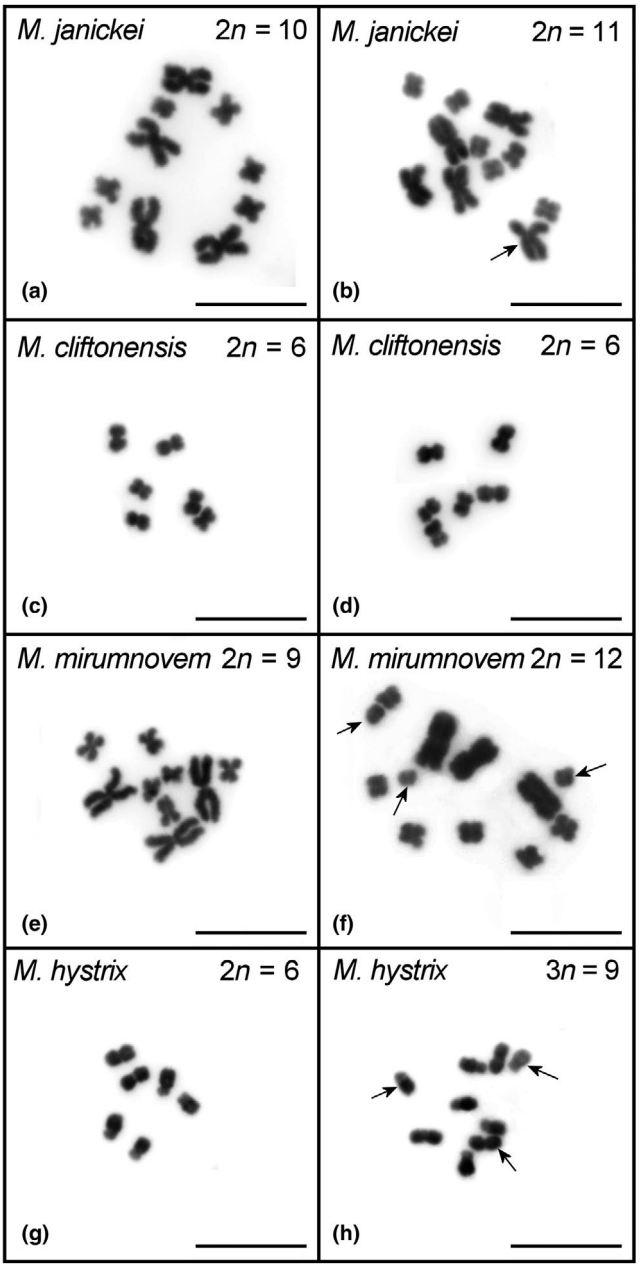

FIGURE 11 Metaphase karyotype spreads of the three new *Macrostomum* species and the outgroup species: (a) the "normal" and most common chromosome set of *M. janickei*; (b) an "abnormal" chromosome set of *M. janickei*; (c-d) two chromosome sets of karyologically uniform *M. cliftonensis*; (e) the "normal" and most common chromosome set of *M. mirumnovem*; (f) one of the many possible "abnormal" chromosome sets of *M. mirumnovem*; (g) the "normal" and almost uniform chromosome set of *M. hystrix*; and (h) a very rare polyploid karyotype variant of *M. hystrix*. Additional chromosomes are marked by arrows. Inverted DAPI image. Scale bar 10 μm

to solely the 2n = 8 karyotype (the other karyotypes are rare in LS1; Zadesenets et al., 2016). These peaks have relative fluorescence values that, respectively, average 3.07x, 3.89x, and 4.69× that of *D. melanogaster*, so that the 2n = 8, 2n = 9, and 2n = 10 karyotypes, corresponding to haploid genome sizes of 525, 666, and 803 Mbp, respectively. However, note that the large chromosomes appear to represent near identical copies (Zadesenets, Schärer, et al., 2017b; Zadesenets et al., 2016), so that the actual amount of unique genome sequence might correspond that observed in the 2n = 8 karyotype.

Earlier results suggested that *M. hystrix* has a stable 2n = 6 karyotype (10/10), with six similar-sized chromosomes (Figure 11g), including two metacentrics and four submetacentrics (Zadesenets et al., 2016). As part of this study, we analyzed an additional 67 worms, which overall confirms this karyotype for almost all specimens (i.e., 75/77, or 97%). However, we also found two specimens with an apparently triploid 3n = 9 karyotype (Figure 11h), with three

metacentrics and six submetacentrics. Shifts from diploidy to triploidy could result from polyspermy (Snook, Hosken, & Karr, 2011; Toda & Okamoto, 2016), which might occur since this species mates by hypodermic insemination (Ramm, Schlatter, Poirier, & Schärer, 2015; Schärer et al., 2011). The notion that *M. hystrix* has a simple karyotype was also supported by our flow cytometric genome size estimates (Figure S1), which showed a single peak having a relative fluorescence that was on average 1.27× that of *D. melanogaster*, corresponding to a haploid genome size in *M. hystrix* of 217 Mbp.

Molecular phylogenetic placements

The topology of the *28S rRNA* gene tree supported three clades among these *M. lignano* relatives (Figure 12), containing (a) *M. janickei* (from France) and *M. lignano* (from Italy and Greece), (b) *M. cliftonensis* (from Western Australia), and (c) *M. mirumnovem* (from Victoria) and an undescribed *Macrostomum* sp. (from South Australia). Note that the latter specimen was collected by Laumer and Giribet (2014) at a site that is ~450 km from our Victoria collection site. Moreover, the tree topology further suggested that this marker is not variable enough to resolve the interrelationships in the first clade, showing a maximum divergence of only 4% among the in-group species. So while the marker is informative for more deeply diverged species (Schärer et al., 2011), more variable markers are needed to resolve these close species.

We therefore used the faster evolving partial *COI* gene, which showed a maximum divergence of close to 20% among the in-group species. The topology of the *COI* gene tree recovered the same three clades, but in addition it also supported a separation between *M. janickei* and the *M. lignano* specimens (Figure 13). Moreover, while all *M. lignano* fall into one supported clade, which we expected given their stylet morphology (Ladurner et al., 2005), there is some substructure among the *M. lignano* specimens from Italy and Greece, with all Italian specimens forming a single well-supported clade, while the Greek specimens from the LS3 line fall into two somewhat separate and poorly supported groups. The LS3 culture was established from collections in two sites on the Sithonia peninsula (i.e., Vourvourou and Porto Koufo; Zadesenets et al., 2016), which lie about 30 km apart. We had not expected population differentiation between those sites, and so the laboratory cultures were established with individuals from both sample sites. It would be interesting to resample these sites to understand if these two *COI* gene sequences map, respectively, onto the two sample sites, or if both populations contain multiple *COI* gene sequences.

Frameshift mutation in the *COI* gene of *Macrostomum hystrix*

The observed frameshift mutation in the *COI* gene was surprising and required further validation. We first confirmed that this deletion was supported by both sequencing directions in both analyzed *M. hystrix* specimens, which stem from two different sampling locations in Italy that are about 300 km apart (Table 1). Next, we confirmed that the deletion was also supported when mapping 10.49 million 101 bp Illumina reads from an RNA-Seq study of the SR1 line of *M. hystrix* (J. N. Brand, & L. Schärer, unpublished data) onto the partial *COI* gene of the SR1 line (using Bowtie2 with local alignment and high sensitivity). In total, 37'921 (0.36%) reads mapped to this fragment, and 3,518 (0.034%) reads mapped to the AAT codon resulting from the deletion, of which 99.9% supported the deletion. This high number of mapped reads clearly suggested that the *COI* gene carrying the deletion is expressed in *M. hystrix* and that it is unlikely that we are dealing with a nuclear pseudogene. To evaluate this further, we used the analogous mapping approach in *M. lignano*, which does not carry the deletion. Specifically, we mapped 12.24 million 100 bp Illumina reads from an RNA-Seq study of the DV1 line of *M. lignano* (Ramm et al., 2019) onto the partial *COI* gene of the DV1 line. In total, 36'710 (0.30%) reads mapped to this fragment, and 5,401 (0.044%) reads mapped to the same codon (which, in the absence of the deletion is an AAA), of which 99.7% supported that codon and thus the absence of a deletion in *M. lignano*.

These results suggest that there are no highly expressed transcripts that lack the deletion in *M. hystrix* (as could have been expected if a version lacking the deletion existed and was expressed, or if RNA editing were to efficiently correct the deletion). Moreover, it seems that the transcript in *M. hystrix* (carrying the deletion) is expressed at a similar level to the transcript in *M. lignano* (not carrying a deletion). Together, this clearly suggests that *M. hystrix* is able to develop, grow and reproduce successfully in spite of the presence of this frameshift mutation. Interestingly, the remainder of the *COI* gene sequence of *M. hystrix* did not show an evidently higher level of divergence, as could have been expected if selection were relaxed after the stop codon. This may suggest that this part of the sequence is still under stabilizing selection, possibly due to residual protein being produced due to translational misreading of the mutant mRNA, as has been shown in other organisms (Andersson, Slechta, & Roth, 1998; Atkins, Elseviers, & Gorini, 1972; Remacle, Gloire, Cardol, & Matagne, 2004). Based upon the new insights presented here, including the above RNA-Seq data, we have now been able to effect a correction of the deposited GenBank sequence to include the deletion (now KP730561.2; see also Table 1).

4 | CONCLUSIONS

We here have identified and taxonomically described three previously undescribed species of the free-living flatworm genus *Macrostomum*, all of which we show to be close relatives of the widely used flatworm model species *M. lignano*. Moreover, all of these newly described species permit to address interesting evolutionary research questions in their own right. First, we show that *M. janickei* is the closest known relative of *M. lignano*, with which it shares an unusual hidden polyploidy. This karyotype organization is likely the result of a whole-genome duplication event via auto-polyploidization, leading to a fusion chromosome that varies considerably in copy number, both within and between these two species (Zadesenets, Ershov, et al., 2017a; Zadesenets, Schärer, et al., 2017b; Zadesenets et al., 2016). This

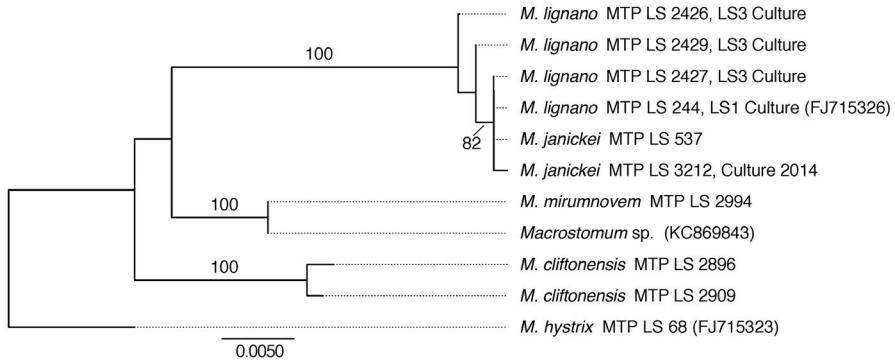

FIGURE 12 Molecular phylogeny of the relatives of *Macrostomum lignano* based on the partial *28S rRNA* gene sequence. The nodal values are bootstrap supports from a Tamura-Nei neighbor joining tree reconstruction (showing only bootstrap values >75%)

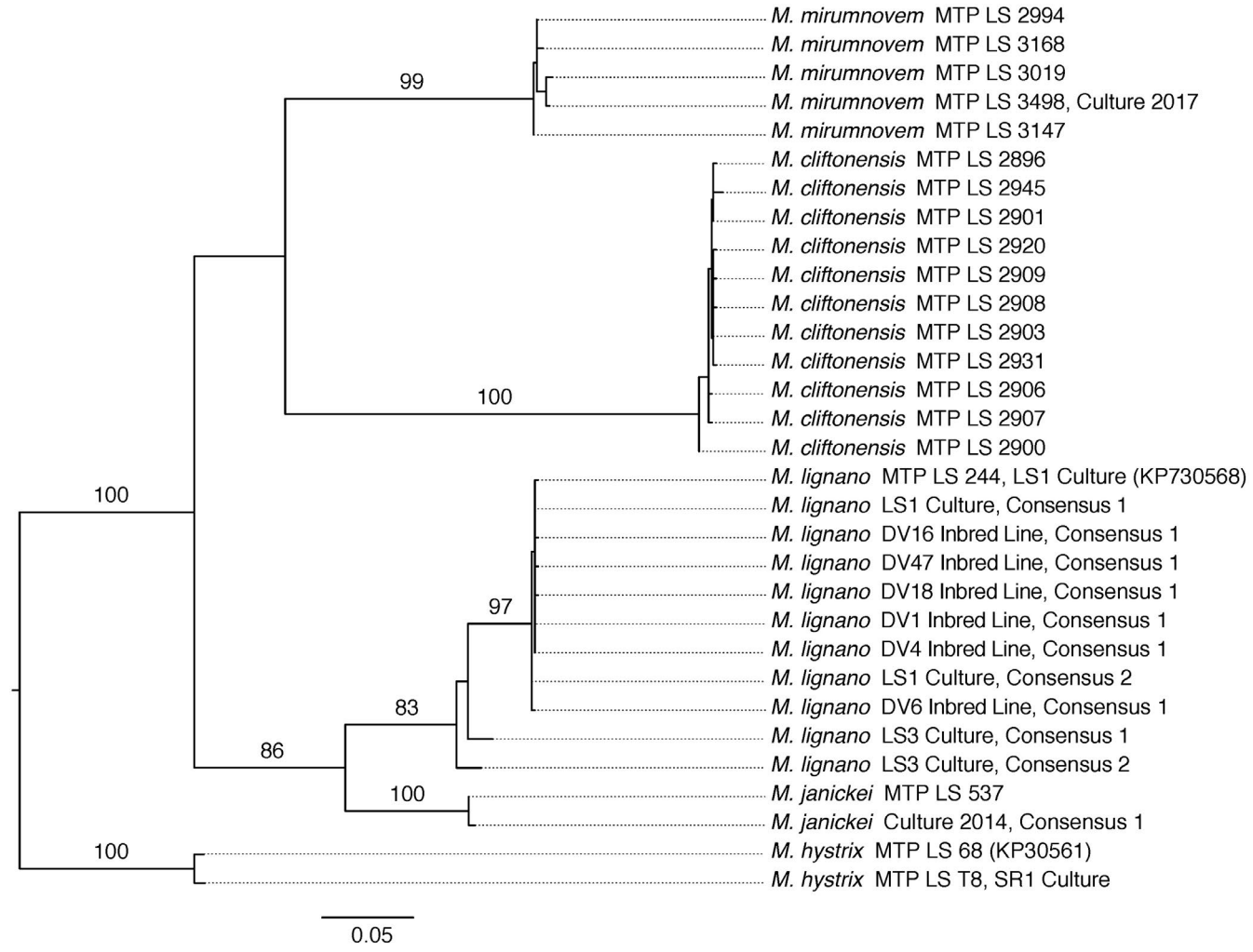

FIGURE 13 Molecular phylogeny of the relatives of *Macrostomum lignano* based on the partial *COI* gene. The nodal values are bootstrap supports from a maximum likelihood tree reconstruction (showing only bootstrap values >75%)

species pair therefore permits to study the evolutionary outcomes of early rediploidization processes following a whole-genome duplication (K. S. Zadesenets, I. E. Jetybayev, L. Schärer, & N. B. Rubtsov, unpublished data), shedding light on processes of genome evolution. Second, *M. mirumnovem* shows an even more unusual genome organization with a 2n = 9 base karyotype pattern, which we think may have resulted via allo-polyploidization (K. S. Zadesenets, I. E. Jetybayev, L. Schärer, & N. B. Rubtsov, unpublished data), and it represents another interesting species to study genome evolution. Moreover, the karyotype variation observed in these *Macrostomum* species calls for studies on gene regulation and dosage compensation. And third, *M. cliftonensis* shows a simple and stable karyotype, and a small haploid genome size of only 231 Mbp, which makes *M. cliftonensis* an attractive species to develop as a genetic and genomic *Macrostomum* model to eventually replace *M. lignano*, particularly since it is also outcrossing and shows the typical reproductive traits of a reciprocally

mating species (Schärer et al., 2011). In addition to describing these new species, we have also shown *M. hystrix* to have a simple and stable karyotype, and a comparably small genome of 217 Mbp, making this a promising model to study the evolution of reproduction in hypodermically mating species (Schärer et al., 2011), particularly since it is currently the closest described relative of *M. lignano* showing that type of mating behavior. Our results showcase the striking biological diversity in *Macrostomum* flatworms, which will permit an even broader range of evolutionary research questions to be addressed in this fascinating genus.

ACKNOWLEDGEMENTS

Tim Janicke and Georgina Rivera-Ingraham; John Evans, Leigh Simmons, and Ben Byrne; and Yvonne Gilbert and Rod Watson, provided support with collecting *M. janickei*, *M. cliftonensis*, and *M. mirumnovem*, respectively. *M. cliftonensis* was collected and exported based on DPAW Reg 17 (01-000135-2) and Reg 18 Licenses (OS002550), respectively. *M. mirumnovem* was collected based on DELWP National Parks Act 1975 Permit (10008144). Dita Vizoso and Anaïs Galli helped with establishing cultures. Eduard Stöckli; Andrew Hosie; and Genefor Walker-Smith and Melanie Mackenzie, kindly received and catalogued specimens for the Natural History Museum Basel, Western Australian Museum and the Museum Victoria, respectively. Manuel Ruedi and Richard Pyle kindly gave advice on questions concerning taxonomy. Maria Pichler and Peter Stadler provided technical assistance with flow cytometry. KZ was supported by project 0324-2019-0042. This research was funded by SNF projects 31003A-143732 and 31003A-162543 to LS.

ORCID

Lukas Schärer https://orcid.org/0000-0002-0209-9871

REFERENCES

Andersson, D. I., Slechta, E. S., & Roth, J. R. (1998). Evidence that gene amplification underlies the adaptive mutability of the *lac* operon. *Science*, *282*, 1133–1135.

Arbore, R., Sekii, K., Beisel, C., Ladurner, P., Berezikov, E., & Schärer, L. (2015). Positional RNA-Seq identifies candidate genes for phenotypic engineering of sexual traits in *Macrostomum lignano*. *Frontiers in Zoology*, *12*, 14. https://doi.org/10.1186/s12983-015-0106-0

Atkins, J. F., Elseviers, D., & Gorini, L. (1972). Low activity of β-galactosidase in frameshift mutants of *Escherichia coli*. *Proceedings of the National Academy of Sciences of the United States of America*, *69*(5), 1192–1195.

Ax, P. (1956). Les turbellariés des étangs côtiers du littoral méditerranéen de la France méridionale. *Vie Et Milieu, Suppl.*, *5*, 1–215.

Ax, P. (1959). Zur Systematik, Ökologie und Tiergeographie der Turbellarienfauna in den ponto-kaspischen Brackwassermeeren. *Zoologische Jahrbücher: Abteilung Für Systematik, Ökologie Und Geographie Der Tiere*, *87*, 43–187.

Ax, P. (1994). *Macrostomum magnacurvituba* n. sp. (Macrostomida, Plathelminthes) replaces *Macrostomum curvituba* in coastal waters of Greenland and Iceland. *Microfauna Marina*, *9*, 335–338.

Ax, P. (2008). *Plathelminthes aus Brackgewässern der Nordhalbkugel*. Stuttgart, Germany: Franz Steiner Verlag.

Bazakos, C., Hanemian, M., Trontin, C., Jiménez-Gómez, J. M., & Loudet, O. (2017). New strategies and tools in quantitative genetics: How to go from the phenotype to the genotype. *Annual Review of Plant Biology*, *68*, 435–455. https://doi.org/10.1146/annurev-arplant-042916-040820

Brooks, A. K., & Gaj, T. (2018). Innovations in CRISPR technology. *Current Opinion in Biotechnology*, *52*, 95–101. https://doi.org/10.1016/j.copbio.2018.03.007

Cardona, A., Hartenstein, V., & Romero, R. (2005). The embryonic development of the triclad *Schmidtea polychroa*. *Development Genes and Evolution*, *215*(3), 109–131.

Egger, B., Bachmann, L., & Fromm, B. (2017). Atp8 is in the ground pattern of flatworm mitochondrial genomes. *BMC Genomics*, *18*, 414. https://doi.org/10.1186/s12864-017-3807-2

Egger, B., Gschwentner, R., Hess, M. W., Nimeth, K. T., Adamski, Z., Willems, M., … Salvenmoser, W. (2009). The caudal regeneration blastema is an accumulation of rapidly proliferating stem cells in the flatworm *Macrostomum lignano*. *BMC Developmental Biology*, *9*, 41. https://doi.org/10.1186/1471-213X-9-41

Egger, B., & Ishida, S. (2005). Chromosome fission or duplication in *Macrostomum lignano* (Macrostomorpha, Plathelminthes) - Remarks on chromosome numbers in 'archoophoran turbellarians'. *Journal of Zoological Systematics and Evolutionary Research*, *43*(2), 127–132. https://doi.org/10.1111/j.1439-0469.2005.00300.x

Egger, B., Ladurner, P., Nimeth, K., Gschwentner, R., & Rieger, R. (2006). The regeneration capacity of the flatworm *Macrostomum lignano*—on repeated regeneration, rejuvenation, and the minimal size needed for regeneration. *Development Genes and Evolution*, *216*(10), 565–577. https ://doi.org/10.1007/s00427-006-0069-4

Faubel, A., & Cameron, B. (2001). Platyhelminthes from salt marshes of Coomera River, Southeastern Queensland, Australia. *Memoirs of the Queensland Museum*, *46*, 511–519.

Gamo, J., & Leal-Zanchet, A. M. (2004). Freshwater microturbellarians (Platyhelminthes) from Rio Grande do Sul, Brazil. *Revista Brasileira De Zoologia*, *21*(4), 897–903. https://doi.org/10.1590/S0101-81752004000400026

Gregory, T. R. (2019). Animal genome size database. http://www.genomesize.com

Grudniewska, M., Mouton, S., Simanov, D., Beltman, F., Grelling, M., de Mulder, K., … Berezikov, E. (2016). Transcriptional signatures of somatic neoblasts and germline cells in Macrostomum lignano. *eLife*, *5*, e20607. https://doi.org/10.7554/eLife.20607

Janicke, T., & Schärer, L. (2010). Sperm competition affects sex allocation but not sperm morphology in a flatworm. *Behavioral Ecology and Sociobiology*, *64*, 1367–1375. https://doi.org/10.1007/s00265-010-0951-y

Janssen, T., Vizoso, D. B., Schulte, G., Littlewood, D. T. J., Waeschenbach, A., & Schärer, L. (2015). The first multi-gene phylogeny of the Macrostomorpha sheds light on the evolution of sexual and asexual reproduction in basal Platyhelminthes. *Molecular Phylogenetics and Evolution*, *92*, 82–107. https://doi.org/10.1016/j.ympev.2015.06.004

Kalyaanamoorthy, S., Minh, B. Q., Wong, T. K. F., von Haeseler, A., & Jermiin, L. S. (2017). ModelFinder: Fast model selection for accurate phylogenetic estimates. *Nature Methods*, *14*, 587–589. https://doi.org/10.1038/nmeth.4285

Kuales, G., De Mulder, K., Glashauser, J., Salvenmoser, W., Takashima, S., Hartenstein, V., … Ladurner, P. (2011). Boule-like genes regulate male and female gametogenesis in the flatworm *Macrostomum lignano*. *Developmental Biology*, *357*, 117–132. https://doi.org/10.1016/j.ydbio.2011.06.030

Ladurner, P., Egger, B., De Mulder, K., Pfister, D., Kuales, G., Salvenmoser, W., & Schärer, L. (2008). The stem cell system of the basal flatworm

Macrostomum lignano. In T. C. G. Bosch (Ed.), *Stem cells: From Hydra to Man* (pp. 75–94). Berlin, Germany: Springer.

Ladurner, P., Schärer, L., Salvenmoser, W., & Rieger, R. M. (2005). A new model organism among the lower Bilateria and the use of digital microscopy in taxonomy of meiobenthic Platyhelminthes: *Macrostomum lignano*, n. sp. (Rhabditophora, Macrostomorpha). *Journal of Zoological Systematics and Evolutionary Research*, *43*(2), 114–126. https://doi.org/10.1111/j.1439-0469.2005.00299.x

Lane, J. A. K., Clarke, A. G., & Winchcombe, Y. C. (2017). *South West Wetlands Monitoring Program 1977–2016*. Perth, WA: Government of Western Australia. Retrieved from https://www.dpaw.wa.gov.au/management/wetlands/wetlands-monitoring-and-research

Laumer, C. E., & Giribet, G. (2014). Inclusive taxon sampling suggests a single, stepwise origin of ectolecithality in Platyhelminthes. *Biological Journal of the Linnean Society*, *111*, 570–588. https://doi.org/10.1111/bij.12236

Lengerer, B., Hennebert, E., Flammang, P., Salvenmoser, W., & Ladurner, P. (2016). Adhesive organ regeneration in *Macrostomum lignano*. *BMC Developmental Biology*, *16*, 20. https://doi.org/10.1186/s12861-016-0121-1

Lengerer, B., Pjeta, R., Wunderer, J., Rodrigues, M., Arbore, R., Schärer, L., … Ladurner, P. (2014). Biological adhesion of the flatworm *Macrostomum lignano* relies on a duo-gland system and is mediated by a cell type-specific intermediate filament protein. *Frontiers in Zoology*, *11*, 12. https://doi.org/10.1186/1742-9994-11-12

Lengerer, B., Wunderer, J., Pjeta, R., Carta, G., Kao, D., Aboobaker, A., … Ladurner, P. (2018). Organ specific gene expression in the regenerating tail of *Macrostomum lignano*. *Developmental Biology*, *433*(2), 448–460. https://doi.org/10.1016/j.ydbio.2017.07.021

Luther, A. (1947). Untersuchungen an rhabdocoelen Turbellarien VI. *Macrostomiden Aus Finnland*. *Acta Zoologica Fennica*, *49*, 1–38.

Marie-Orleach, L., Janicke, T., & Schärer, L. (2013). Effects of mating status on copulatory and postcopulatory behaviour in a simultaneous hermaphrodite. *Animal Behaviour*, *85*(2), 453–461. https://doi.org/10.1016/j.anbehav.2012.12.007

Marie-Orleach, L., Janicke, T., Vizoso, D. B., David, P., & Schärer, L. (2016). Quantifying episodes of sexual selection: Insights from a transparent worm with fluorescent sperm. *Evolution*, *70*(2), 314–328. https://doi.org/10.1111/evo.12861

Marie-Orleach, L., Janicke, T., Vizoso, D. B., Eichmann, M., & Schärer, L. (2014). Fluorescent sperm in a transparent worm: Validation of a GFP marker to study sexual selection. *BMC Evolutionary Biology*, *14*, 148. https://doi.org/10.1186/1471-2148-14-148

Mouton, S., Grudniewska, M., Glazenburg, L., Guryev, V., & Berezikov, E. (2018). Resilience to aging in the regeneration-capable flatworm *Macrostomum lignano*. *Aging Cell*, *17*(3), e12739. https://doi.org/10.1111/acel.12739

Mouton, S., Willems, M., Braeckman, B. P., Egger, B., Ladurner, P., Schärer, L., & Borgonie, G. (2009). The free-living flatworm *Macrostomum lignano*: A new model organism for ageing research. *Experimental Gerontology*, *44*, 243–249. https://doi.org/10.1016/j.exger.2008.11.007

Newmark, P. A., & Sánchez Alvarado, A. (2002). Not your father's planarian: A classic model enters the era of functional genomics. *Nature Reviews Genetics*, *3*(3), 210–219. https://doi.org/10.1038/nrg759

Nguyen, L.-T., Schmidt, H. A., Haeseler, A. V., & Minh, B. Q. (2015). IQ-TREE: A fast and effective stochastic algorithm for estimating maximum-likelihood phylogenies. *Molecular Biology and Evolution*, *32*(1), 268–274. https://doi.org/10.1093/molbev/msu300

Papi, F. (1951). Richerche sui Turbellari Macrostomidae. *Archivo Zoologico Italiano*, *36*, 289–341.

Papi, F. (1953). Beiträge zur Kenntnis der Macrostomiden (Turbellarien). *Acta Zoologica Fennica*, *78*, 1–32.

Pellettieri, J., & Sánchez Alvarado, A. (2007). Cell turnover and adult tissue homeostasis: From humans to planarians. *Annual Review of Genetics*, *41*, 83–105. https://doi.org/10.1146/annurev.genet.41.110306.130244

Pfister, D., De Mulder, K., Hartenstein, V., Kuales, G., Borgonie, G., Marx, F., … Ladurner, P. (2008). Flatworm stem cells and the germ line: Developmental and evolutionary implications of macvasa expression in *Macrostomum lignano*. *Developmental Biology*, *319*(1), 146–159. https://doi.org/10.1016/j.ydbio.2008.02.045

Ramm, S. A., Lengerer, B., Arbore, R., Pjeta, R., Wunderer, J., Giannakara, A., … Schärer, L. (2019). Sex allocation plasticity on a transcriptome scale: Socially sensitive gene expression in a simultaneous hermaphrodite. *Molecular Ecology*, *28*(9), 2321–2341. https://doi.org/10.1111/mec.15077

Ramm, S. A., Schlatter, A., Poirier, M., & Schärer, L. (2015). Hypodermic self-insemination as a reproductive assurance strategy. *Proceedings of the Royal Society B-Biological Sciences*, *282*, 20150660. https://doi.org/10.1098/rspb.2015.0660

Remacle, C., Gloire, G., Cardol, P., & Matagne, R. F. (2004). Impact of a mutation in the mitochondrial LSU rRNA gene from Chlamydomonas reinhardtii on the activity and the assembly of respiratory-chain complexes. *Current Genetics*, *45*, 323–330. https://doi.org/10.1007/s00294-004-0490-z

Rink, J. C. (2013). Stem cell systems and regeneration in planaria. *Development Genes and Evolution*, *223*(1–2), 67–84. https://doi.org/10.1007/s00427-012-0426-4

Rouhana, L., Weiss, J. A., Forsthoefel, D. J., Lee, H., King, R. S., Inoue, T., … Newmark, P. A. (2013). RNA interference by feeding in vitro–synthesized double-stranded RNA to planarians: Methodology and dynamics. *Developmental Dynamics*, *242*, 718–730. https://doi.org/10.1002/dvdy.23950

Schärer, L., Joss, G., & Sandner, P. (2004). Mating behaviour of the marine turbellarian *Macrostomum* sp.: These worms *suck*. *Marine Biology*, *145*, 373–380. https://doi.org/10.1007/s00227-004-1314-x

Schärer, L., Littlewood, D. T. J., Waeschenbach, A., Yoshida, W., & Vizoso, D. B. (2011). Mating behaviour and the evolution of sperm design. *Proceedings of the National Academy of Sciences of the United States of America*, *108*(4), 1490–1495. https://doi.org/10.1073/pnas.1013892108

Sekii, K., Vizoso, D. B., Kuales, G., De Mulder, K., Ladurner, P., & Schärer, L. (2013). Phenotypic engineering of sperm-production rate confirms evolutionary predictions of sperm competition theory. *Proceedings of the Royal Society B-Biological Sciences*, *280*(1757), 20122711. https://doi.org/10.1098/rspb.2012.2711

Singh, P., Vellnow, N., & Schärer, L. (2019). Variation in sex allocation plasticity in three closely related flatworm species. *Ecology and Evolution*. https://doi.org/10.1002/ece3.5566

Snook, R. R., Hosken, D. J., & Karr, T. L. (2011). The biology and evolution of polyspermy: Insights from cellular and functional studies of sperm and centrosomal behavior in the fertilized egg. *Reproduction*, *142*, 779–792. https://doi.org/10.1530/REP-11-0255

Stelzer, C.-P., Riss, S., & Stadler, P. (2011). Genome size evolution at the speciation level: The cryptic species complex *Brachionus plicatilis* (Rotifera). *BMC Evolutionary Biology*, *11*, 90. https://doi.org/10.1186/1471-2148-11-90

Telford, M. J., Herniou, E. A., Russell, R. B., & Littlewood, D. T. J. (2000). Changes in mitochondrial genetic codes as phylogenetic characters: Two examples from the flatworms. *Proceedings of the National Academy of Sciences of the United States of America*, *97*(21), 11359–11364. https://doi.org/10.1073/pnas.97.21.11359

Toda, E., & Okamoto, T. (2016). Formation of triploid plants via possible polyspermy. *Plant Signaling & Behavior*, *11*(9), e1218107. https://doi.org/10.1080/15592324.2016.1218107

Vellnow, N., Vizoso, D. B., Viktorin, G., & Schärer, L. (2017). No evidence for strong cytonuclear conflict over sex allocation in a simultaneously hermaphroditic flatworm. *BMC Evolutionary Biology*, *17*, 103. https://doi.org/10.1186/s12862-017-0952-9

Wasik, K. A., Gurtowski, J., Zhou, X., Mendivil Ramos, O., Delás, M. J., Battistoni, G., … Schatz, M. C. (2015). Genome and transcriptome of the regeneration-competent flatworm, *Macrostomum lignano*. *Proceedings of the National Academy of Sciences of the United States of America*, *112*(40), 12462–12467. https://doi.org/10.1073/pnas.1516718112

Wudarski, J., Simanov, D., Ustyantsev, K., de Mulder, K., Grelling, M., Grudniewska, M., … Berezikov, E. (2017). Efficient transgenesis and annotated genome sequence of the regenerative flatworm model *Macrostomum lignano*. *Nature Communications*, *8*, 2120. https://doi.org/10.1038/s41467-017-02214-8

Wunderer, J., Lengerer, B., Pjeta, R., Bertemes, P., Kremser, L., Lindner, H., … Ladurner, P. (2019). A mechanism for temporary bioadhesion. *Proceedings of the National Academy of Sciences*, *116*(10), 4297–4306. https://doi.org/10.1073/pnas.1814230116

Young, J. O. (1972). Further studies on the occurrence of freshwater Microturbellaria in the British Isles. I. A description of *Macrostomum johni* sp. nov. *Freshwater Biology*, *2*, 253–258. https://doi.org/10.1111/j.1365-2427.1972.tb00054.x

Young, J. O. (1976). Systematic studies of limnic *Macrostomum* species (Turbellaria, Macrostomida) from East Africa. *Zoologica Scripta*, *5*, 49–60.

Zadesenets, K. S., Ershov, N. I., Berezikov, E., & Rubtsov, N. B. (2017a). Chromosome evolution in the free-living flatworms: First evidence of intrachromosomal rearrangements in karyotype evolution of *Macrostomum lignano* (Platyhelminthes, Macrostomida). *Genes*, *8*, 298. https://doi.org/10.3390/genes8110298

Zadesenets, K. S., Schärer, L., & Rubtsov, N. B. (2017b). New insights into the karyotype evolution of the free-living flatworm *Macrostomum lignano* (Platyhelminthes, Turbellaria). *Scientific Reports*, *7*, 6066. https://doi.org/10.1038/s41598-017-06498-0

Zadesenets, K. S., Vizoso, D. B., Schlatter, A., Konopatskaia, I. D., Berezikov, E., Schärer, L., & Rubtsov, N. B. (2016). Evidence for karyotype polymorphism in the free-living flatworm, *Macrostomum lignano*, a model organism for evolutionary and developmental biology. *PLoS ONE*, *11*(10), e0164915. https://doi.org/10.1371/journal.pone.0164915

SUPPORTING INFORMATION

Additional supporting information may be found online in the Supporting Information section at the end of the article.

Figure S1 Flow-cytometric measurements of genome size in five *Macrostomum* species (*M. lignano*, *M. janickei*, *M. cliftonensis*, *M. mirumnovem*, and *M. hystrix*), including three different lines/cultures of *M. lignano* (the inbred line DV1, and the outbred cultures LS1 and LS3), with 2–4 replicates per species (rows).

Table S1 Primers used for PCR amplification and sequencing of the analysed partial *28S rRNA* and *COI* gene sequences.

Alignment S1 Alignment of the partial *28S rRNA* gene sequences (FASTA-format).

Alignment S2 Alignment of the partial *COI* gene sequences (FASTA-format).

Video S1 Video sequence of mating behaviour of *Macrostomum janickei* n. sp., showing circling, copulation and suck behaviour.

Video S2 Video sequence of mating behaviour of *Macrostomum cliftonensis* n. sp., showing circling, copulation and suck behaviour.

Video S3 Video sequence of mating behaviour of *Macrostomum mirumnovem* n. sp., showing circling, copulation and suck behaviour.

How to cite this article: Schärer L, Brand JN, Singh P, Zadesenets KS, Stelzer C-P, Viktorin G. A phylogenetically informed search for an alternative *Macrostomum* model species, with notes on taxonomy, mating behavior, karyology, and genome size. *J Zool Syst Evol Res*. 2019;00:1–25. https://doi.org/10.1111/jzs.12344